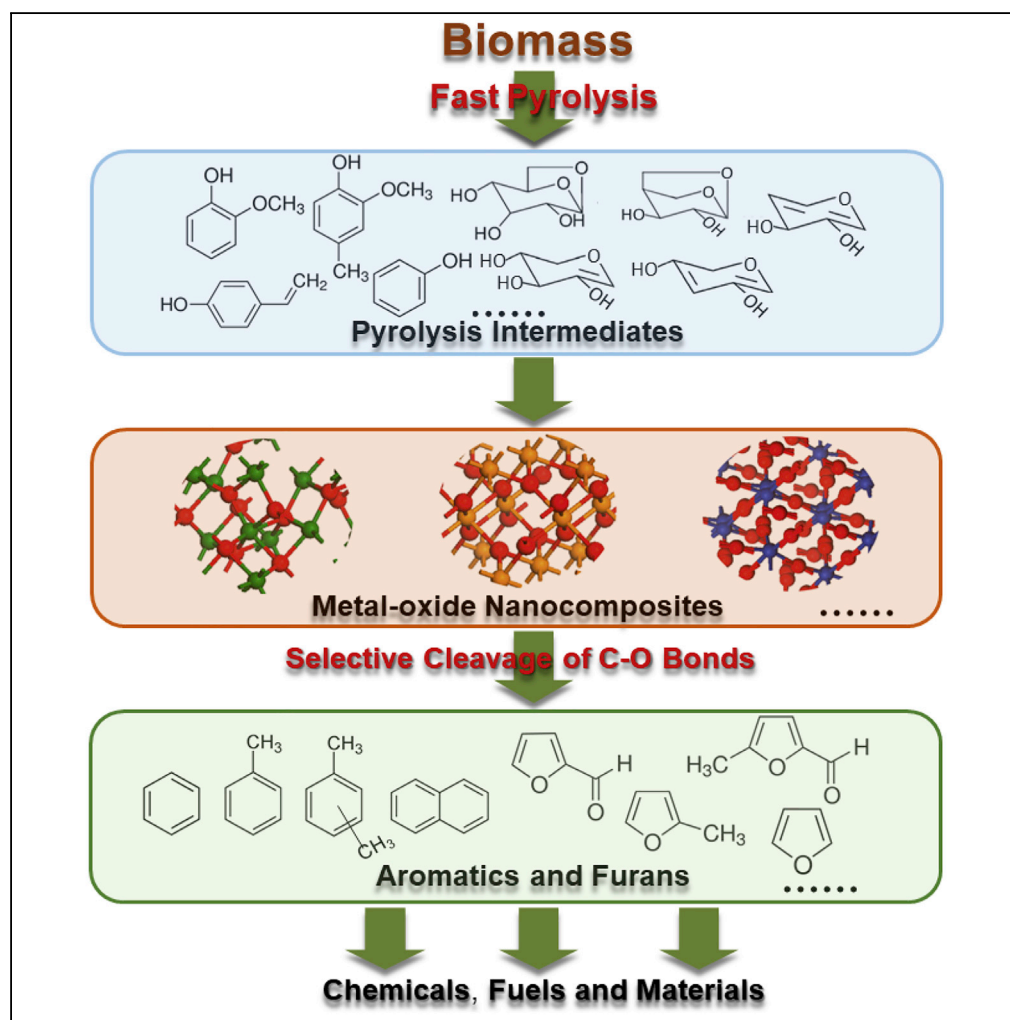


Article

Controlling Deoxygenation Pathways in Catalytic Fast Pyrolysis of Biomass and Its Components by Using Metal-Oxide Nanocomposites



Anqing Zheng,
Zhen Huang,
Guoqiang Wei, ...,
Zengli Zhao,
Yuanyu Tian,
Haibin Li

zhaozl@ms.giec.ac.cn (Z.Z.)
tianyuy1008@126.com (Y.T.)

HIGHLIGHTS

WO₃-TiO₂-Al₂O₃ (WTA)
can selectively break the
C-O bonds within biomass

Lignin and
polysaccharides are
respectively converted
into aromatics and furans

Brønsted and Lewis acid
sites of WTA are
responsible for the C-O
bond cleavages

Zheng et al., iScience 23,
100814
January 24, 2020 © 2019 The
Author(s).
[https://doi.org/10.1016/
j.isci.2019.100814](https://doi.org/10.1016/j.isci.2019.100814)

Article

Controlling Deoxygenation Pathways in Catalytic Fast Pyrolysis of Biomass and Its Components by Using Metal-Oxide Nanocomposites

Anqing Zheng,^{1,2,3,4,5} Zhen Huang,^{2,4,5} Guoqiang Wei,^{2,4,5} Kun Zhao,^{2,4,5} Liqun Jiang,^{2,4,5} Zengli Zhao,^{2,4,5,6,*} Yuanyu Tian,^{1,*} and Haibin Li^{2,4,5}

SUMMARY

Selectively breaking the C-O bonds within biomass during catalytic fast pyrolysis (CFP) is desired, but extremely challenging. Herein, we develop a series of metal-oxide nanocomposites composed of W, Mo, Zr, Ti, or Al. It is demonstrated that the nanocomposites of WO_3 - TiO_2 - Al_2O_3 exhibit the highest deoxygenation ability during CFP of lignin, which can compete with the commercial HZSM-5 catalyst. The nanocomposites can selectively cleave the C-O bonds within lignin-derived phenols to form aromatics by direct demethoxylation and subsequent dehydration. Moreover, the nanocomposites can also achieve the selective breaking of the C-O bonds within xylan and cellulose to form furans by dehydration. The Brønsted and Lewis acid sites on the nanocomposites can be responsible for the deoxygenation of lignin and polysaccharides, respectively. This study provides new insights for the rational design of multifunctional catalysts that are capable of simultaneously breaking the C-O bonds within lignin and polysaccharides.

INTRODUCTION

With the increasing societal concerns regarding fossil fuel shortages and climate change, lignocellulosic biomass has emerged as a potential alternative to fossil fuels for the production of chemicals and liquid fuels (Custodis et al., 2014; Huber et al., 2006; Liu et al., 2015; Meng et al., 2017; Rahimi et al., 2014; Roman-Leshkov et al., 2007). Lignocellulosic biomass generally consists of three major components: hemicellulose, cellulose, and lignin. Lignin is an amorphous, cross-linked heteropolymer composed of three phenylpropane units that vary in their degree of methoxylation: sinapyl, coniferyl, and *p*-coumaryl alcohol (Li et al., 2015a; Liu et al., 2016; Wang et al., 2015b). Cellulose and hemicellulose, the most typical structural polysaccharides, are polymers composed of six-carbon and five-carbon sugar units, typically glucose and xylose (Patwardhan et al., 2010, 2011; Wang et al., 2017). The pre-existing aromatic structures of lignin and the pyranose/furanose ring structures of polysaccharides tend to render them very suitable for the production of aromatics and furans, respectively. However, one fundamental challenge is that both the lignin and polysaccharides are highly oxygen-rich when compared with their respective platform chemicals (aromatics and furans) (Kusumoto and Nozaki, 2015; Shiramizu and Toste, 2012) (as shown in Figure 1).

The C-O bonds within lignin, hemicellulose, and cellulose exist in very different chemical environments. The major oxygen-containing functional groups within lignin are aryl ethers, methoxyls, hydroxyls (phenolic and aliphatic), and carbonyls (Wang et al., 2009). The oxygen within cellulose and hemicellulose exists predominantly in the forms of aliphatic ethers (glycosidic bond) and aliphatic hydroxyls (Li et al., 2012). The deoxygenation of biomass proceeds by the cleavage of the C-O and C-C bonds. The former comprises dehydration (the elimination of H_2O) and demethoxylation (the elimination of CH_3OH), whereas the latter consists of decarbonylation (the elimination of CO) and decarboxylation (the elimination of CO_2) (Dayton et al., 2015). The deoxygenation of biomass via decarbonylation and decarboxylation can cause unnecessary carbon losses, resulting in a reduction in both the liquid yield and energy recovery. Hence, selectively and simultaneously breaking the C-O bonds present in the different chemical environments is crucial to achieving the efficient deoxygenation of biomass. Recently, oxophilic metals have exhibited promising activities and selectivities for the cleavage of the C-O bonds within biomass

¹State Key Laboratory of Heavy Oil Processing, China University of Petroleum (East China), Qingdao, Shandong 266580, China

²Guangzhou Institute of Energy Conversion, Chinese Academy of Sciences, Guangzhou 510640, PR China

³Shenzhen Huazhong University of Science and Technology Research Institute, Shenzhen 523000, PR China

⁴CAS Key Laboratory of Renewable Energy, Guangzhou 510640, PR China

⁵Guangdong Key Laboratory of New and Renewable Energy Research and Development, Guangzhou 510640, PR China

⁶Lead Contact

*Correspondence: zhaozl@ms.giec.ac.cn (Z.Z.), tianyy1008@126.com (Y.T.)
<https://doi.org/10.1016/j.isci.2019.100814>



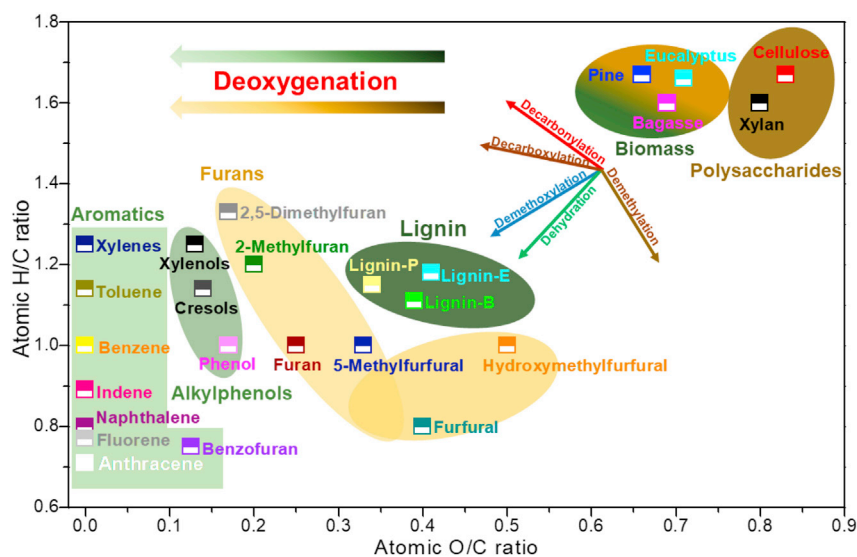


Figure 1. The van Krevelen Diagram of Feedstocks and Their Respective Target Products

The organosolv lignin derived from pine, eucalyptus, and bagasse is denoted lignin-P, lignin-E, and lignin-B, respectively.

through the strong interactions between the oxygen-containing functional groups and the oxophilic metal (Chen et al., 2018b; Robinson et al., 2016; Wan et al., 2018). Wang and coworkers reported that the simultaneous hydrodeoxygenation of cellulose, hemicellulose, and lignin into hexane, pentane, and alkylcyclohexanes could be achieved by a multifunctional Pt/NbOPO₄ catalyst under solvothermal conditions (Xia et al., 2016). Lu demonstrated that Re₂O₇ can selectively cleave the C-O bonds within lignin (Qi et al., 2018). Sanna reported that the catalytic pyrolysis of biomass over activated olivine and activated serpentine was able to reduce the oxygen content of bio-oil by up to 40% (Sanna and Andréßen, 2012). Shanks, Nimlos, and Román-Leshkov showed that the pyrolysis vapors from biomass can be hydrodeoxygenated to form alkanes and aromatics using MoO₃ or supported MoO₃ under H₂ atmosphere (Murugappan et al., 2016; Nolte et al., 2016).

Despite these advances, there remains a challenge in designing a multifunctional catalyst capable of simultaneously converting lignin, hemicellulose, and cellulose into their respective aromatics and furans by deoxygenation reactions. Catalytic fast pyrolysis (CFP) is one of the most promising methods to directly convert biomass into highly deoxygenated molecules over catalysts at middle temperature (450°C–650°C), high heating rate (>1,000°C/s), short reaction time (several seconds), and atmospheric pressure without the need for a H₂ supply (Carlson et al., 2008; Li et al., 2015b; Wang et al., 2009, 2014; Zhang et al., 2009a). The deactivated solid catalysts can be recycled after burning off the coke in a regenerator. Currently, renewable aromatics can be produced by the CFP of biomass over various zeolite catalysts, such as HZSM-5, H β , HY, HUSY, MCM-41, FCC, and hierarchical zeolites (Du et al., 2013; Iliopoulou et al., 2012; Jae et al., 2011; Jia et al., 2017; Kelkar et al., 2015; Wang et al., 2014, 2018; Zhang et al., 2013). HZSM-5 has exhibited the highest aromatic yield due to its strong acidity and shape selectivity (Cheng et al., 2012). During the CFP of biomass over zeolites, the first step is the thermally induced cleavage of the C-C and C-O bonds within the entire biomass to generate various pyrolysis intermediates (e.g., anhydrosugars, furans, phenols, alcohol, aldehydes, and ketones). The pyrolysis intermediates subsequently diffuse into the pore channels of the zeolite and further undergo a variety of cracking, deoxygenation, oligomerization, cyclization, and aromatization reactions at the Brønsted acid sites to form olefins and aromatics via hydrocarbon pool mechanism (Carlson et al., 2011; Hoff et al., 2017; Yang et al., 2017; Zhang et al., 2009b). In addition, renewable furans (e.g., furfural) can be produced by CFP. Blasi and Lu have shown Lewis acids, such as Fe₂(SO₄)₃ and ZnCl₂, to be the most effective catalysts for the selective production of furfural from the fast pyrolysis of corn cob (Branca et al., 2012; Lu et al., 2011). Hence, a catalyst comprising both Brønsted and Lewis acid sites could be a suitable candidate for the coproduction of aromatics and furans from the CFP of biomass. Lewis acidity appears in γ -Al₂O₃, γ -Ga₂O₃, and TiO₂. Brønsted acidity exists in oxides of elements with formal valences higher than four (WO₃, MoO₃, V₂O₅, Nb₂O₅, and S-containing oxides) (Fernández-García and Rodriguez, 2011).

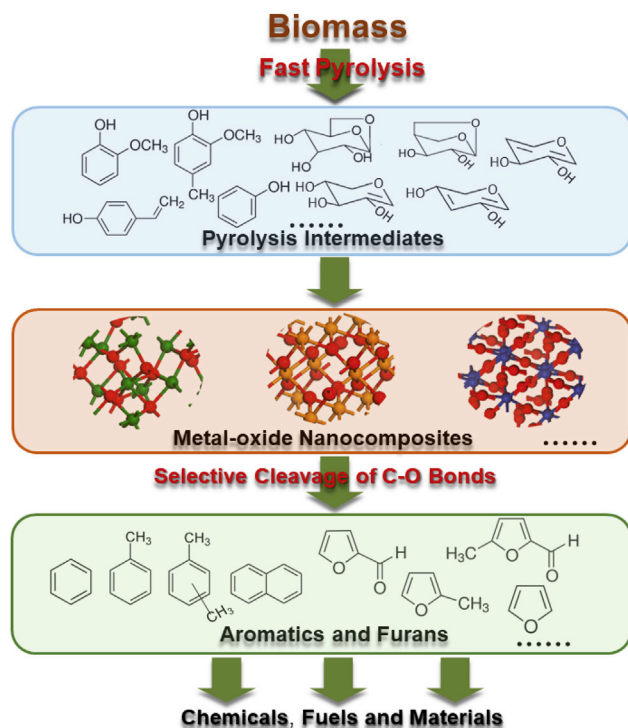


Figure 2. The Proposed Pyrolytic Strategy for Producing Aromatics and Furans from Biomass

Here, we propose a new pyrolytic strategy for the production of value-added chemicals and platform chemicals from biomass (as shown in Figure 2). The CFP of three main components of biomass (organosolv lignin, xylan, and cellulose) over metal-oxide nanocomposites is first investigated for catalyst screening. Then the performance of the CFP of real biomass (bagasse, eucalyptus, and pine) over the metal-oxide nanocomposites was verified. It is found that lignin and polysaccharides can be, respectively, converted into aromatics and furans over the metal-oxide nanocomposites composed of W, Ti, and Al. The nanocomposites can selectively break the C-O bonds within lignin-derived phenols to generate aromatics by direct demethoxylation and dehydration reactions, and they can also selectively cleave the C-O bonds within xylan and cellulose to form furans by dehydration reactions. The Brønsted and Lewis acid sites of the nanocomposites may be responsible for the deoxygenation of lignin and polysaccharides, respectively.

RESULTS AND DISCUSSION

Synthesis and Characterization of the Metal-Oxide Nanocomposites

The metal-oxide nanocomposites, e.g., $\text{TiO}_2\text{-Al}_2\text{O}_3$ (TA), $\text{ZrO}_2\text{-Al}_2\text{O}_3$ (ZA), $\text{ZrO}_2\text{-TiO}_2$ (ZT), $\text{WO}_3\text{-TiO}_2\text{-Al}_2\text{O}_3$ (WTA), $\text{WO}_3\text{-ZrO}_2\text{-Al}_2\text{O}_3$, $\text{MO}_3\text{-TiO}_2\text{-Al}_2\text{O}_3$ (MTA), and $\text{WO}_3\text{-ZrO}_2\text{-TiO}_2$ were prepared using a coprecipitation method (see “Transparent Methods” for preparation and characterization). The acronyms in parentheses are formed by combining the initial letters of these metal oxides. Transmission electron microscopic images (Figures 3A–3C) show that the average sizes of TA, WTA, and MTA samples are estimated to be 12.9, 10.8, and 9.9 nm, respectively. The X-ray diffraction (XRD) patterns of TA, WTA, and MTA are shown in Figure 3D. It is evident that the three samples have very similar XRD patterns. The diffraction peaks at $2\theta = 25.2^\circ, 37.8^\circ, 48.1^\circ, 54.0^\circ, 55.1^\circ, 62.8^\circ, 68.9^\circ, 70.4^\circ,$ and 75.2° are assigned to the reflections from the (101), (004), (200), (105), (211), (204), (116), (220), and (215) crystal planes of anatase TiO_2 (JCPDS No. 21-1272), respectively (Chen et al., 2018a). The small diffraction peaks at $37.1^\circ, 45.8^\circ,$ and 66.8° are attributed to the reflections from the (311), (400), and (440) crystal planes of $\gamma\text{-Al}_2\text{O}_3$ (JCPDS No.29-0063), respectively (Xiong et al., 2019). No independent peaks corresponding to the crystalline planes of WO_3 or MO_3 are observed in the XRD patterns of WTA and MTA, indicating that the incorporated WO_3 and MO_3 are dispersed homogeneously over the TiO_2 and Al_2O_3 supports and exist in poorly crystalline and amorphous forms. The concentrations of Brønsted and Lewis acid sites on the metal-oxide nanocomposites are given in Figure 3E. Only small quantities of Lewis acid sites are found in nano- TiO_2 (T), whereas both Brønsted and

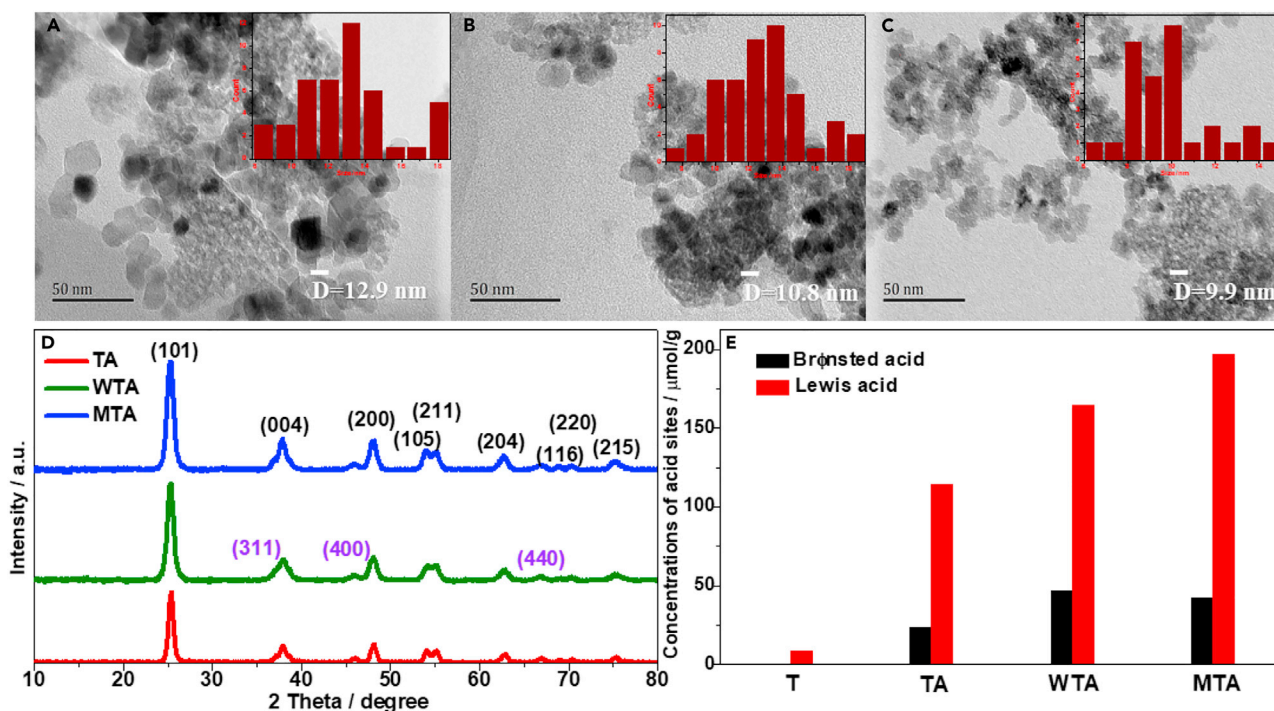


Figure 3. Characterization of the Metal-Oxide Nanocomposites

(A–C) Transmission electron microscopic images of (A) TA, (B) WTA, and (C) MTA.

(D) Powder XRD patterns of TA, WTA, and MTA.

(E) The concentrations of acid sites in T, TA, WTA, and MTA.

Lewis acid sites are observed in TA, WTA, and MTA. The rank order for the concentrations of Brønsted acid sites is $WTA > MTA > TA > T$, whereas the rank order for the concentrations of Lewis acid sites is $MTA > WTA > TA > T$. It is generally accepted that the oxygen vacancies exposed on the surface of metal-oxide nanocomposites supply coordinatively unsaturated metal cations that act as Lewis acid sites. The interaction with water converts the surface oxygens of the metal-oxide nanocomposites into hydroxyl groups, and the hydrogens in the hydroxyl groups behave as Brønsted acid sites (Guntida et al., 2019; Kim et al., 2019; Koodali, 2006). As WTA as an example, interaction of the tungsten species with the surface of TiO_2 or Al_2O_3 (wetting phenomenon) can result in the formation of surface mono-oxo wolframyl groups with coordinatively unsaturated structure, which act as strong Lewis acid sites. As a result of adsorption of water, the coordination number of tungsten increases and the site behaves as a strong Brønsted acid site (Cristiani et al., 1993; Guntida et al., 2019; Gutiérrez-Alejandre et al., 1998). It is thus concluded that the mono-oxo wolframyl groups and hydrated wolframyl groups on the surface of WTA are, respectively, responsible for the formation of strong Lewis and Brønsted acid sites.

Catalytic Fast Pyrolysis of Lignin over the Nanocomposites

Organosolv lignin derived from bagasse was selected as the feedstock. The major products from the CFP of the organosolv lignin include various methoxyphenols, non-methoxyphenols, aromatics, char/coke, and permanent gas. In this study, we mainly focus on the formation of target products: monophenols (methoxyphenols and non-methoxyphenols) and aromatics. Methoxyphenols are defined as a class of compounds that comprise one or more methoxy groups (OCH_3) directly bound to the aromatic ring in phenols. Non-methoxyphenols are defined as a class of monophenols without methoxy groups. The non-methoxyphenols from the fast pyrolysis of organosolv lignin without the use of nanocomposites are mainly composed of alkenylphenols (mainly vinyl, propenyl, and allyl phenols), phenol, and alkylphenols (mainly cresols, ethylphenols, and xylenols). Herein, nanoscale TiO_2 (T), ZrO_2 (Z), and Al_2O_3 (A) are used as catalysts in the CFP of organosolv lignin. However, no aromatics are observed in the pyrolysis products. Surprisingly, it is found that the metal-oxide nanocomposites, TA, ZA, and ZT, are able to produce aromatics and non-methoxyphenols. The non-methoxyphenols from CFP consist of phenol and alkylphenols (mainly cresols,

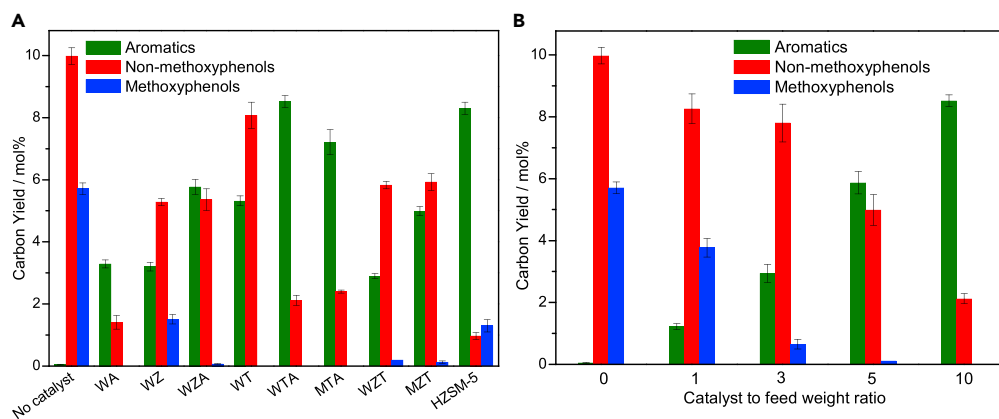


Figure 4. The Carbon Yields of Aromatics and Phenols from the CFP of Organosolv Lignin Derived from Bagasse at 600°C

(A and B) (A) CFP over different nanocomposites with a catalyst-to-feedstock weight ratio of 10 and (B) CFP over WTA with different catalyst-to-feedstock weight ratios, where no catalyst is denoted as a catalyst-to-feedstock weight ratio of 0.

ethylphenols, xylenols, ethyl cresols, and trimethylphenols). The aromatics comprise benzene, toluene, xylenes, alkylbenzenes, naphthalenes, benzofurans, indenes, anthracenes, fluorenes, and phenanthrenes. As shown in Figure S1, the rank order for the aromatic yield is TA > ZT > ZA. The aromatic yield from the CFP of lignin can be further improved by the introduction of WO_3 (W) and MoO_3 (M) into the Zr-, Ti-, or Al-based nanocomposites. It is well known that the metal-oxide nanocomposites of WO_3 , MoO_3 , ZrO_2 , TiO_2 , or Al_2O_3 are robust solid acidic catalysts with high thermal stabilities (Barton et al., 1998). As shown in Figure 4A, WTA and MTA exhibit the best catalytic performance of the nanocomposites in terms of their deoxygenation abilities. The aromatic yields from the CFP of lignin over WTA are close to those over HZSM-5, indicating that these catalysts can compete with HZSM-5 in the CFP of lignin. It should be noted that no aromatics are found during the CFP of lignin over T. The catalysts produce aromatics when Al_2O_3 is incorporated into T. Further incorporation of WO_3 or MO_3 into TA enhances the aromatic yield. The results suggest that the rank order for the deoxygenation activities appears to be the same as the concentrations of Brønsted acid sites present in the nanocomposites. The aromatic selectivity from the CFP of lignin over the different nanocomposites is shown in Figure S2. WZ, MTA, and WTA show the highest selectivities toward benzene, toluene, and xylenes (BTX). A significant proportion of alkylaromatics, especially alkylbenzenes, are formed via alkylation reactions during the CFP of lignin. Among the nanocomposites, WT exhibits the best performance in terms of alkylation.

The effects of the catalyst-to-feedstock weight ratio on the carbon yields of the aromatics and phenols from the CFP of lignin are illustrated in Figure 4B. The yields of aromatics, methoxyphenols, and non-methoxyphenols are dependent upon the catalyst-to-feedstock weight ratio, indicating that the extent of deoxygenation during CFP of lignin, that is, the selectivity toward aromatics, methoxyphenols, or non-methoxyphenols, can be readily tuned by controlling the catalyst-to-feedstock weight ratio. As the catalyst-to-feedstock weight ratio increases from 0 to 10, the yields of the methoxyphenols and non-methoxyphenols decrease, whereas the yields of the aromatics significantly increase. The results are in accordance with the CFP of lignin over zeolites (Jan et al., 2015; Kim et al., 2015; Luo et al., 2019). It should be noted that the sum of the yields of the methoxyphenols, non-methoxyphenols, and aromatics decreases with increasing catalyst-to-feedstock weight ratio. These results may be due to the increased severities of deoxygenation in the hydrogen-deficient environments of CFP promoting hydrogen transfer reactions. As shown in Figure S3, the carbon yields of char/coke from the CFP of organosolv lignin are approximately 50%–71%. The results are in line with those in literatures, which reported that the carbon yields of char/coke and permanent gas from the CFP of biomass over zeolites or metal oxides were 30%–75% and 20%–50%, respectively (Carlson et al., 2011; Murugappan et al., 2016; Wang et al., 2015a).

Possible Reaction Pathways for the Catalytic Fast Pyrolysis of Lignin

In the CFP of lignin, the first step is the thermal depolymerization of lignin to form various phenols. The main oxygen-containing groups in these phenols are phenolic hydroxyl and methoxy groups. These

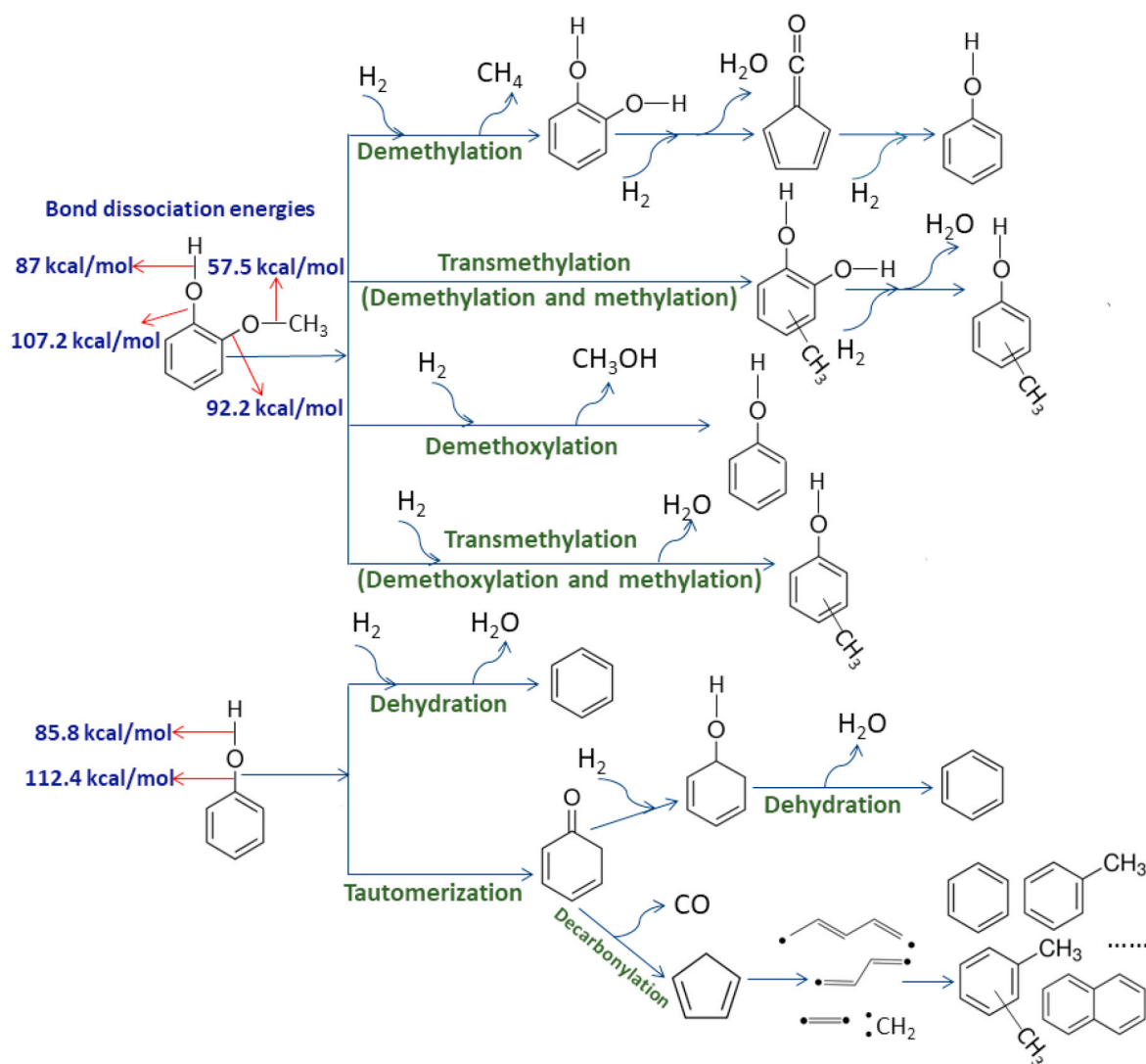


Figure 5. The Bond Dissociation Energies for Typical Bonds within Phenol and Guaiacol, and the Possible Pathways for the Catalytic Conversion of Phenol and Guaiacol into Aromatics

phenols subsequently diffuse onto the catalyst surface to undergo deoxygenation reactions. As shown in Figure 5, the deoxygenation of phenol to form benzene can proceed by three distinct pathways: the tautomerization-dehydration and tautomerization-decarbonylation routes starting from the cleavage of the O-H bond and a direct dehydration route via the breaking of the C_{aryl}-OH bond (Lup et al., 2017; Rogers and Zheng, 2016; Teles et al., 2018). There are four generally accepted pathways for removing the methoxy group from guaiacol: (1) cleavage of the O-CH₃ bond to produce methane (demethylation) and catechol, (2) transmethylation reactions that can be considered to be the results of demethylation of guaiacol and subsequent methylation of catechol, (3) splitting of the C_{aryl}-OCH₃ bond to produce methanol (demethoxylation) and phenol, and (4) transmethylation reactions that can be considered to be the results of demethoxylation of guaiacol and subsequent methylation of phenol (Rogers and Zheng, 2016). The bond dissociation energies for O-H, C_{aryl}-OH, O-CH₃, and C_{aryl}-OCH₃ in guaiacol are 87.0, 107.2, 57.5, and 97.2 kcal/mol, respectively (Kubiak, 1995; Schlaf and Zhang, 2015; Vuori and Bredenbergh, 1987). Although the bond dissociation energies can change by 1–10 kcal/mol between double substituted benzenes (e.g., guaiacol) and mono-substituted benzenes (e.g., phenol), the rank order of the bond dissociation energies is approximately the same: O-CH₃ < O-H < C_{aryl}-OCH₃ < C_{aryl}-OH. The higher bond dissociation energies of the C_{aryl}-OCH₃ and C_{aryl}-OH bonds make their preferential cleavage very difficult to achieve.

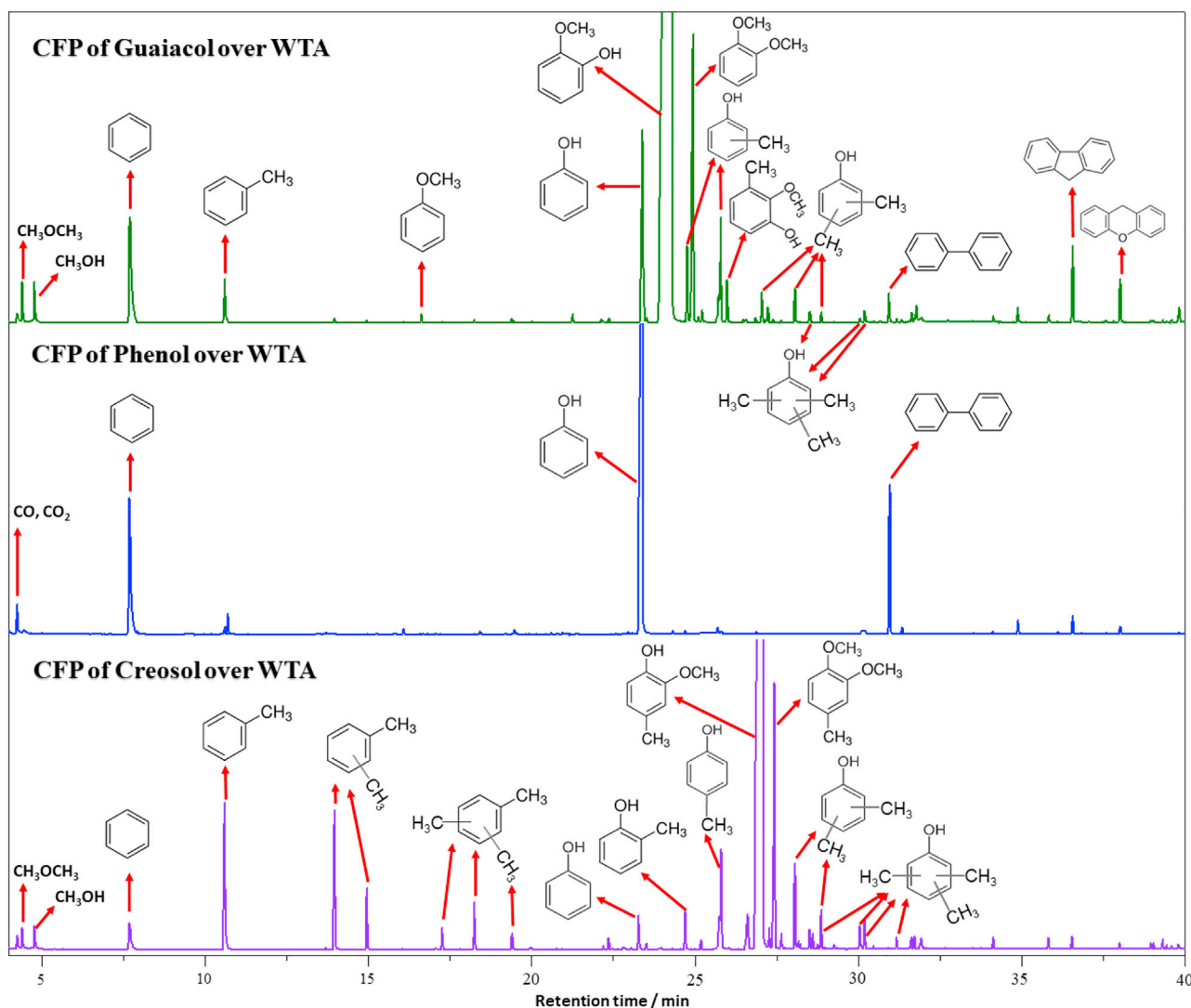


Figure 6. Total Ion Chromatograms Resulting from the CFP of Guaiacol, Phenol, and Creosol over WTA at 600°C with a Catalyst-to-Feedstock Weight Ratio of 5

To further understand the reaction mechanism of the CFP of lignin over the nanocomposites, phenol, guaiacol, and creosol are selected as probe molecules to identify the possible pathways. The total ion chromatograms resulting from the CFP of guaiacol, phenol, and creosol over WTA are shown in Figure 6. The major products from the CFP of guaiacol are 1,2-dimethoxy benzene, cresols, creosol, phenol, benzene, toluene, xylenols, methanol, dimethyl ether (DME), biphenyl, fluorene, xanthene, and trimethylphenols. Very small amounts of CO and CO₂ are also observed in the product stream, indicating that decarbonylation and decarboxylation are not the primary reactions that occur during the CFP of guaiacol. Large amounts of 1,2-dimethoxy benzene, cresols, creosol, xylenols, and trimethylphenols present in the product stream indicate that the transmethylation reaction is one of the major reactions during CFP. There are only two possible pathways for the formation of transmethylation products: (1) demethylation and subsequent methylation and (2) demethoxylation and subsequent methylation (as shown in Figure 5). Considerable quantity of phenol and the very small quantity of anisole present in the product stream imply that demethoxylation is the initiating step for the CFP of guaiacol. Catechol is not found from the CFP of guaiacol, suggesting that demethylation is not a predominant reaction pathway during the CFP of guaiacol. The 1,2-dimethoxy benzene, cresols, creosol, xylenols, and trimethylphenol products are presumed to be obtained via the C-methylation and O-methylation of various reactants and intermediates with methanol and

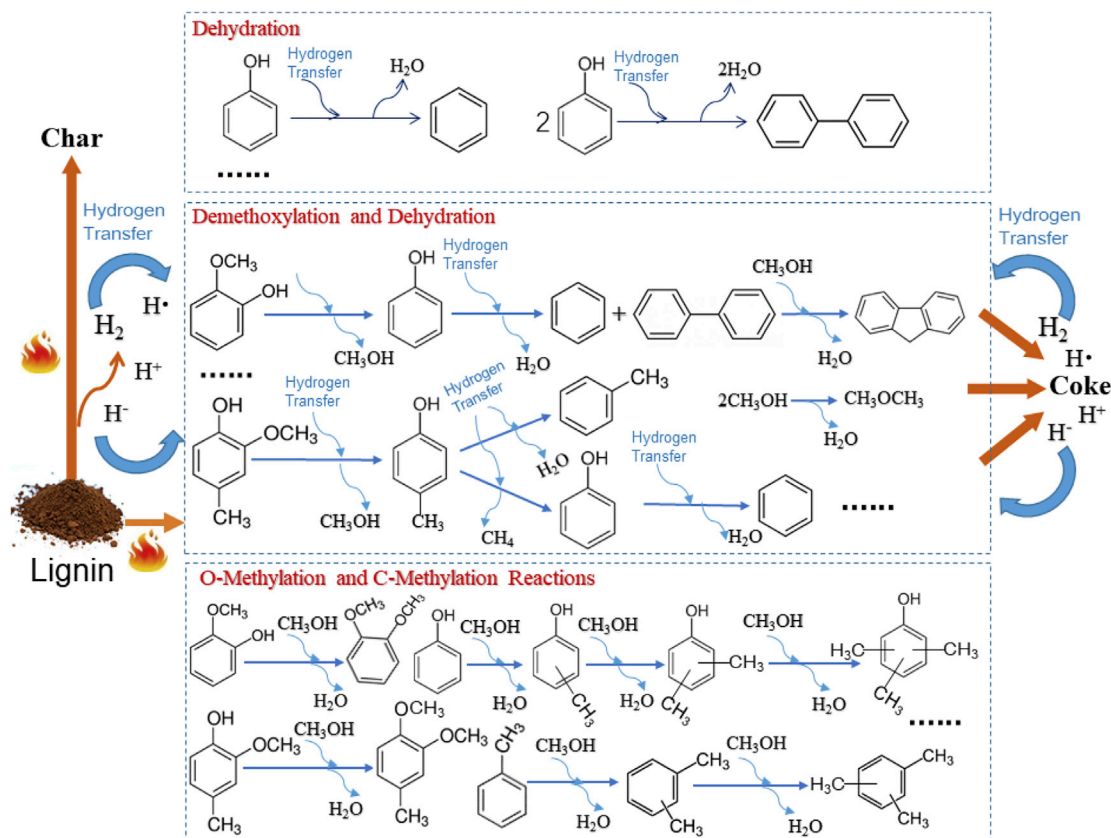


Figure 7. The Possible Pathways for the CFP of Lignin over the Metal-Oxide Nanocomposites

DME over the nanocomposites. The 1,2-dimethoxy benzene is generated by the O-methylation of guaiacol with methanol and DME, whereas the cresols, xylenols, and trimethylphenols are produced by consecutive C-methylation reactions of phenol with methanol and DME. Cooperation of the acid and base sites is typically required for C-methylation and O-methylation reactions (Vishwanathan et al., 2008). As shown in Figure S4, CO₂ desorption confirms the basicity of TA, WTA, and MTA. Toluene is obtained by either the dehydration of cresols or the methylation of benzene with methanol. These C-methylation and O-methylation reactions, taken together with the phenol, methanol, and DME present in the product stream, strongly suggest that direct demethoxylation of guaiacol is the major pathway for the deoxygenation of guaiacol over WTA. The main products from the CFP of cresol include 3,4-dimethoxytoluene, toluene, xylenes, trimethylbenzene, cresols, xylenols, and trimethylphenols. The similar product distribution from the CFP of cresol as that from guaiacol further verifies the proposed mechanism.

The possible pathways for the CFP of lignin are illustrated in Figure 7. It is postulated that the hydrogen transfer reactions that occur during the CFP of lignin eliminate the need for an external hydrogen source. H₂ and active hydrogen species (hydrogen radicals, hydrides, and protons) derived from the dehydrogenation, polycondensation, and carbonization reactions during the CFP of lignin can serve as hydrogen donors to cleave the C-O bonds within the various phenols. The proposed pathways for CFP of guaiacol over WTA are significantly different from those over zeolites. Hemberger and coworkers have reported that fulvenone, generated by the catalytic demethylation and subsequent dehydration of guaiacol, is the central reactive intermediate during the CFP of guaiacol over HUSY (Hemberger et al., 2017). The primary products from the CFP of phenol are benzene and biphenyl, strongly indicating that benzene is mainly formed by the direct dehydration of phenol via a free radical mechanism. Phenol first undergoes homolytic fission of the C_{aryl}-OH bond to form aryl and hydroxyl radicals. The hydrogen radicals are subsequently added to the aryl and hydroxyl radicals to form benzene and water. Biphenyl is generated by the recombination of two aryl radicals. Thilakarathne and coworkers demonstrated that the major products from the CFP of phenol over HZSM-5 are benzene, naphthalene, biphenyl, alkylated naphthalenes, higher polyaromatic hydrocarbons, and olefins. They proposed that the aromatics

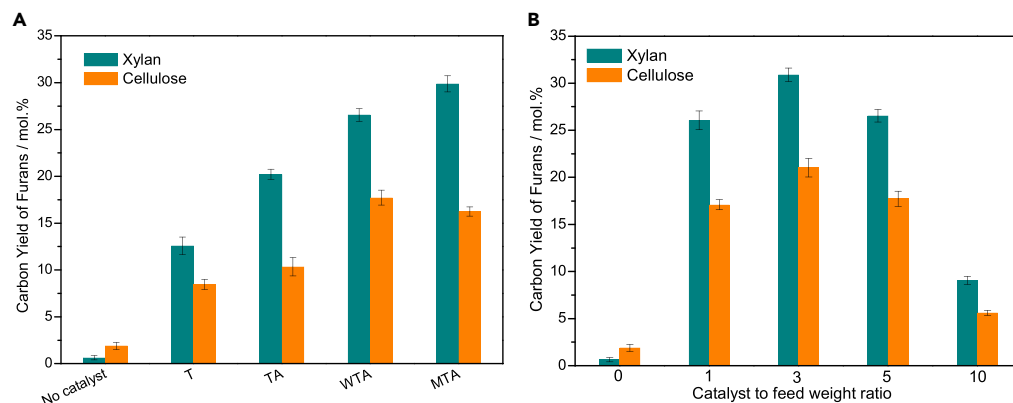


Figure 8. The Carbon Yields of Furans from the CFP of Xylan and Cellulose at 600°C

(A and B) (A) CFP over different nanocomposites with a catalyst-to-feedstock weight ratio of 5 and (B) CFP over WTA with different catalyst-to-feedstock weight ratios, where no catalyst is denoted as a catalyst-to-feedstock weight ratio of 0.

produced from the CFP of phenol over HZSM-5 are generated via both a direct dehydration route and a tautomerization-decarbonylation route, with the latter being the predominant route (Thilakarathne et al., 2016). Olefins are not observed from CFP of phenol, guaiacol, and creosol over WTA. These results strongly suggest that the aromatics are predominantly produced by the direct demethoxylation and dehydration of lignin-derived phenols. However, olefins are detected during CFP of lignin. The olefins may be formed by the removal of alkenyl side chains from alkenylphenols. It is supposed that the nanocomposites are capable of selectively reducing the dissociation energies of the $C_{\text{aryl}}\text{-OCH}_3$ and $C_{\text{aryl}}\text{-OH}$ bonds of the adsorbed phenols. The high temperature present during CFP facilitates the selective cleavage of these bonds (Shao et al., 2017). However, the actual mechanisms for the CFP of lignin are much more complex than those for the CFP of model compounds. Large quantities of polycyclic aromatics are detected during the CFP of lignin over the nanocomposites. These results may be due to the rearrangement, recombination, and polycondensation of various lignin-derived reactive intermediates (e.g., radicals and carbenium ions) during the CFP of lignin (Custodis et al., 2014).

Catalytic Fast Pyrolysis of Hemicellulose and Cellulose over the Nanocomposites

Xylan is selected as a representative of hemicellulose. The CFP of xylan and cellulose are also performed over these nanocomposites. The ion chromatograms resulting from the CFP of xylan and cellulose are graphed in Figure S5. The product distributions from the fast pyrolysis of xylan and cellulose are significantly altered by these nanocomposites. The CFP of xylan and cellulose over these nanocomposites favors the formation of furans. The furans from the CFP of xylan are mainly composed of furfural along with small quantities of furan and 2-methylfuran. In addition to the furans mentioned above, large quantities of 5-methylfurfural are also observed from the CFP of cellulose. In addition, aldehydes, ketones, and carboxylic acids, such as formaldehyde, acetaldehyde, acetone, butanone, 2-methyl-2-cyclopenten-1-one, and acetic acid, are found during the CFP of xylan and cellulose. Furans, aldehydes, and ketones are important precursors for hydrocarbon fuels. No aromatics and olefins are observed from the CFP of xylan and cellulose, suggesting that aromatics cannot be generated over the nanocomposites via hydrocarbon pool mechanism.

The yields of furans from CFP of xylan and cellulose catalyzed by the different nanocomposites are depicted in Figure 8A. These nanocomposites can drastically improve the yields of furans. The maximum carbon yields of furans from xylan (29.9%) and cellulose (17.7%) are achieved by CFP over MTA and WTA, respectively. The rank order of the carbon yields of furans from the CFP of xylan is $\text{MTA} > \text{WTA} > \text{TA} > \text{T}$. The rank order of the deoxygenation activities for xylan appears to be the same as that for the concentration of Lewis acid sites present in the nanocomposites. The carbon yields of furans from the CFP of cellulose are lower than those from the CFP of xylan under the same reaction conditions. The rank order of the carbon yields of furans from the CFP of cellulose is $\text{WTA} > \text{MTA} > \text{TA} > \text{T}$. It is worth noting that T can effectively catalyze the formation of furans from xylan and cellulose, whereas no aromatics are detected during the T-catalyzed CFP of lignin. Considering that T possesses only Lewis acid sites, it can be inferred that the formation of furans and aromatics is catalyzed by Lewis and Brønsted acid sites, respectively. As shown in Figure 9, the carbon yields of furans from the CFP of xylan is a linear function of the concentration of Lewis

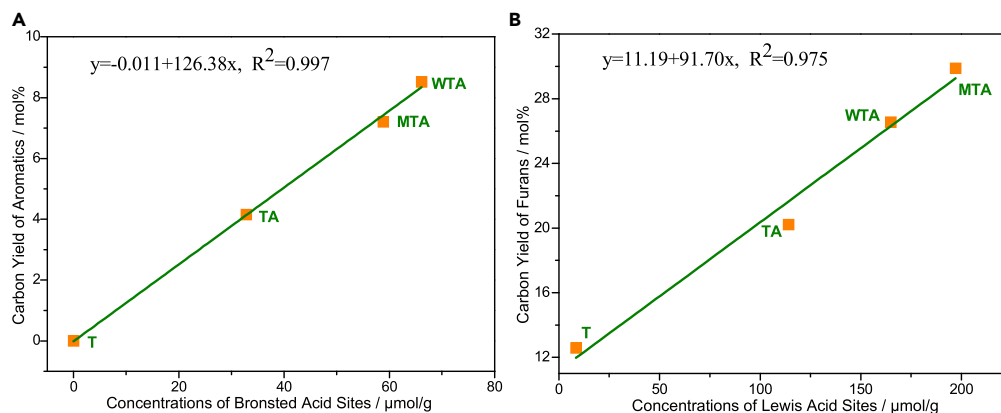


Figure 9. The Carbon Yield of Aromatics or Furans as a Function of the Concentration of Acid Sites

(A) The carbon yield of aromatics from CFP of organosolv lignin as a function of the concentration of Brønsted acid sites. (B) The carbon yield of furans from CFP of xylan as a function of the concentration of Lewis acid sites.

acid sites, whereas the carbon yields of aromatics from the CFP of lignin is a linear function of the concentration of Brønsted acid sites. These results suggest that the formation of furans and aromatics is catalyzed by Lewis and Brønsted acid sites, respectively. The carbon yields of furans as a function of the catalyst-to-feedstock weight ratio are graphed in Figure 8B. The carbon yields of furans reach a maximum value at a catalyst-to-feedstock weight ratio of 3, and then the yields decrease with increasing catalyst-to-feedstock weight ratios. The possible reaction mechanism for the formation of furans from the CFP of xylan and cellulose is shown in Figure S6. It is widely accepted that the first step is the thermal depolymerization of cellulose and xylan to form anhydrosugars (e.g., levoglucosan [LG] and anhydroxylopyranoses [AXP]) through the cleavage of the C-O bonds (glycosidic bonds) (Lin et al., 2009; Liu et al., 2014; Patwardhan et al., 2010, 2011; Shen and Gu, 2009; Wang et al., 2012). LG can undergo dehydration reactions to generate 5-hydroxymethylfurfural, which can undergo subsequent dehydration and decarboxylation reactions to form 5-methylfurfural and 2-methylfuran. 5-Hydroxymethylfurfural can be converted into furfural and formaldehyde by removing the hydroxymethyl group. This result is strongly supported by the fact that formaldehyde is only found in the product stream of the CFP of cellulose. AXP can undergo dehydration reactions to form dianhydroxylopyranoses (DAXP). AXP and DAXP can be further dehydrated to produce furfural. In addition, a small quantity of furans may be derived from glucose and xylose, which can be formed through the acid-catalyzed hydrolysis of cellulose and xylan during CFP.

Catalytic Fast Pyrolysis of Biomass over WTA

Bagasse, eucalyptus, and pine, as representatives of herbaceous, hardwood, and softwood plants, were selected as the feedstocks for CFP. The yields of aromatics and phenols from the CFP of these feedstocks over WTA are given in Figure 10A. WTA is capable of simultaneously converting the polysaccharides and lignin fractions in the different biomass into furans and aromatics, indicating that CFP over WTA is a versatile and feedstock-flexible method for the coproduction of aromatics and furans from biomass. At a catalyst-to-feedstock weight ratio of 5, the maximum carbon yield of furans (20.4%) is achieved by the CFP of the eucalyptus feedstock. Under the same conditions, the CFP of the pine feedstock exhibits the lowest carbon yield of furans (13.0%) and the highest carbon yield of aromatics (10.7%). The results can be ascribed to the different chemical structures of bagasse, eucalyptus, and pine, especially the chemical structures of their hemicellulose and lignin fractions. In softwood plants, galactoglucomannan and guaiacyl units are the major components of the hemicellulose and lignin fractions, respectively. The effects of the catalyst-to-feedstock weight ratios on the product distribution from the CFP of pine feedstock over WTA are illustrated in Figure 10B. The phenols from the fast pyrolysis of pine without the use of the nano-composites are mainly methoxyphenols. As the catalyst-to-feedstock weight ratio increases, the yields of furans and non-methoxyphenols first increase and then begin to decrease as the catalyst-to-feedstock ratio passes 3. The non-methoxyphenols from the CFP of the pine feedstock are mainly phenol and alkylphenols (mainly cresols, ethylphenols, xylenols, ethyl cresols, and trimethylphenols). In addition, the yields of the aromatics gradually increase and reach a maximum value at a catalyst-to-feedstock weight ratio of 10. These results further suggest that the methoxyphenols first undergo demethoxylation reactions to form

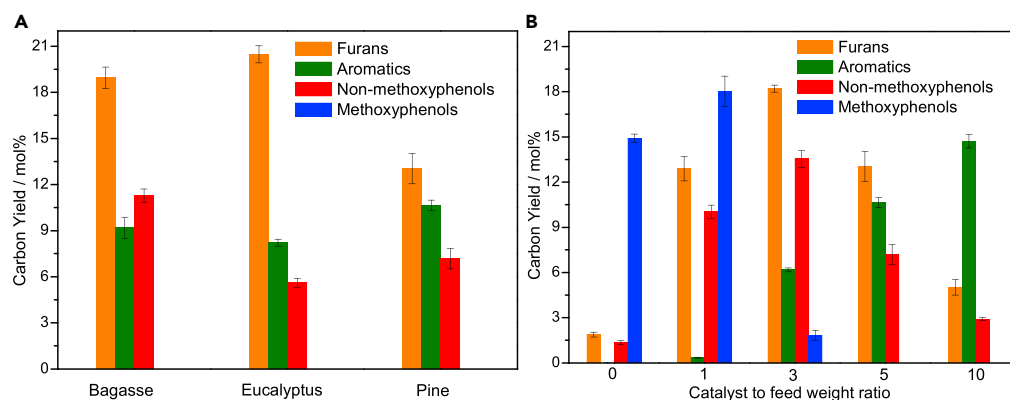


Figure 10. The Carbon Yields of the Furans, Aromatics, and Phenols from the CFP of Raw Biomass over WTA at 600°C

(A and B) (A) CFP of the different feedstocks over WTA with a catalyst-to-feedstock weight ratio of 5 and (B) CFP of the pine feedstock over WTA with varying catalyst-to-feedstock weight ratios, where no catalyst is denoted as a catalyst-to-feedstock weight ratio of 0.

phenol and alkylphenols, which then undergo dehydration reactions to generate aromatics. Also, the yield and selectivity toward aromatics, methoxyphenols or non-methoxyphenols can be tuned by controlling the catalyst-to-feedstock weight ratio. Notably, the sum of the carbon yields of the aromatics, non-methoxyphenols, and methoxyphenols increases significantly from 16.3% to 28.4% when the catalyst-to-feedstock weight ratio increases from 0 to 1. These results are the opposite of those from the CFP of individual lignin over WTA. As shown in Figures 7 and S6, the deoxygenation of phenols requires the hydrogen transfer reactions, in which hydrogen is supplied by the *in situ* dehydrogenation, polycondensation, and carbonization reactions of lignin and phenols. In contrast, the furans are formed by intramolecular dehydration, which does not require an external hydrogen source. It can be hypothesized that the hydrogen transfer reactions between the polysaccharides and lignin are significantly promoted by WTA, resulting in the formation of a greater amount of phenols and aromatics from the CFP of raw biomass via the hydrogenolysis reaction. Lercher reported that the presence of Lewis acid sites in zeolites can enhance both the strength of Brønsted acid sites and the rate of hydrogen transfer reactions (Müller et al., 2016; Wichterlová et al., 1999). Xiao found that the hydrogen transfer reactions between cellulose and lignin occurred during co-fast pyrolysis of cellulose and lignin without any catalysts (Wu et al., 2016). Lignin and polysaccharides typically require different reaction conditions to be completely converted into their respective platform chemicals. The optimal catalyst-to-feedstock weight ratios for maximizing the yields of furans, non-methoxyphenols, and aromatics are 3, 3, and 10, respectively. By comprehensively considering the yields of the furans and aromatics, the optimal catalyst-to-feedstock weight ratio for the CFP of biomass is 3–5. The yield of aromatics and furans from the CFP of biomass and its components over the catalysts reported in the literature are given in Tables S1 and S2 for comparison. As shown in Table S1, the catalysts used in the CFP of biomass for aromatic production include zeolites and mixed metal oxides, such as HZSM-5, modified HZSM-5, and Mo-containing mixed metal oxides, which are well-known strong Brønsted acids (Edmunds et al., 2019; Lu et al., 2019; Murugappan et al., 2016; Wang et al., 2015a). CFP of biomass over different catalysts for furanic production are provided in Table S2. It is found that both Brønsted and Lewis acid catalysts, such as zeolites, H₂SO₄, and ZnCl₂, can effectively catalyze the dehydration of polysaccharides to form furans (Branca et al., 2012; Chen et al., 2018c; Lu et al., 2011). However, the simultaneous conversion of lignin and polysaccharides into respective aromatics and furans has not yet been achieved in the literature. Our results demonstrate that WTA with suitable Brønsted and Lewis acid sites could be the key for achieving efficient and simultaneous deoxygenation of lignin and holocellulose.

Conclusions

Lignocellulosic biomass is a highly heterogeneous polymer, and controlling the complex pyrolysis pathways of this biomass is challenging. Metal-oxide nanocomposites comprising W, Mo, Ti, Zr, or Al are successfully synthesized and applied to simultaneously control the deoxygenation pathways of lignin, cellulose, hemicellulose. The mono-oxo wolframyl groups and hydrated wolframyl groups on surface of WTA act as strong Lewis and Brønsted acid sites, respectively. It is demonstrated that the nanocomposites of

WTA can achieve the selective breaking of the C-O bonds within the lignin-derived phenols to generate aromatics by direct demethoxylation and subsequent dehydration reactions, while also enabling the selective cleavage of the C-O bonds within xylan and cellulose to produce furans by dehydration reactions. Methanol, produced from the direct demethoxylation of lignin-derived pyrolysis intermediates, can further undergo methylation reactions to form alkylated phenols and aromatics. It is inferred that the Brønsted acid sites and Lewis acid sites of the nanocomposites can be responsible for the formation of the aromatics and furans, respectively. Moreover, during the CFP of raw biomass feedstocks, the nanocomposites can promote hydrogen transfer reactions between the polysaccharides and lignin, resulting in the formation of a greater amount of phenols and aromatics. However, the high-temperature and H-deficient environment of CFP can lead to low yields of the target products. To overcome these disadvantages, an additional H₂ supply or low-temperature hydrothermal/solvothermal conditions should be explored in further studies.

Limitations of the Study

The mass balances for CFP of lignin, xylan, cellulose, and biomass are not provided in this study. In addition, the stability and recyclability of the metal-oxide nanocomposites during CFP are also not considered. We will conduct CFP of biomass and its components over metal-oxide nanocomposites in a fixed bed reactor for providing relevant information.

METHODS

All methods can be found in the accompanying [Transparent Methods supplemental file](#).

SUPPLEMENTAL INFORMATION

Supplemental Information can be found online at <https://doi.org/10.1016/j.isci.2019.100814>.

ACKNOWLEDGMENTS

The authors gratefully acknowledge the National Key R&D Program of China (Grant 2017YFE0124200), the National Natural Science Foundation of China (Grants 51776209, 51661145011 and 21406227), the Natural Science Foundation of Shenzhen (JCYJ20170818164006890), the Science and Technology Planning Project of Guangdong Province (2015A020215024), Youth Innovation Promotion Association, CAS (2018383), and Pearl River S&T Nova Program of Guangzhou (Grant 201806010061) for their financial support of this work. The authors also express their sincere thanks to the Analytical and Testing Center of Guangzhou Institute of Energy Conversion, Chinese Academy of Sciences for the assistance of pyrolysis experiments.

AUTHOR CONTRIBUTIONS

A.Z., Z.Z., Y.T., and H.L. conceived of the research and designed the experiments, A.Z. carried out the preparation, characterization, and catalytic fast pyrolysis. A.Z., Z.H., G.W., and K.Z. analyzed and discussed the data; A.Z. wrote the manuscript, and Z.H., G.W., K.Z., L.J., Z.Z., Y.T.; and H.L. discussed and revised the manuscript.

DECLARATION OF INTERESTS

The authors declare no competing interests.

Received: February 25, 2019

Revised: December 4, 2019

Accepted: December 26, 2019

Published: January 24, 2020

REFERENCES

- Barton, D.G., Soled, S.L., and Iglesia, E. (1998). Solid acid catalysts based on supported tungsten oxides. *Top. Catal.* 6, 87–99.
- Branca, C., Di Blasi, C., and Galgano, A. (2012). Catalyst screening for the production of furfural from corncob pyrolysis. *Energy Fuels* 26, 1520–1530.
- Carlson, T.R., Cheng, Y.-T., Jae, J., and Huber, G.W. (2011). Production of green aromatics and olefins by catalytic fast pyrolysis of wood sawdust. *Energy Environ. Sci.* 4, 145–161.
- Carlson, T.R., Vispute, T.P., and Huber, G.W. (2008). Green gasoline by catalytic fast pyrolysis of solid biomass derived compounds. *ChemSusChem* 1, 397–400.
- Chen, M., Ma, J., Zhang, B., Wang, F., Li, Y., Zhang, C., and He, H. (2018a). Facet-dependent performance of anatase TiO₂ for photocatalytic oxidation of gaseous ammonia. *Appl. Catal. B Environ.* 223, 209–215.
- Chen, W.-T., Zhang, Y., Lee, T.H., Wu, Z., Si, B., Lee, C.-F.F., Lin, A., and Sharma, B.K. (2018b). Renewable diesel blendstocks produced by

- hydrothermal liquefaction of wet biowaste. *Nat. Sustain.* **1**, 702–710.
- Chen, X., Chen, Y., Chen, Z., Zhu, D., Yang, H., Liu, P., Li, T., and Chen, H. (2018c). Catalytic fast pyrolysis of cellulose to produce furan compounds with SAPO type catalysts. *J. Anal. Appl. Pyrol.* **129**, 53–60.
- Cheng, Y.-T., Jae, J., Shi, J., Fan, W., and Huber, G.W. (2012). Production of renewable aromatic compounds by catalytic fast pyrolysis of lignocellulosic biomass with bifunctional Ga/ZSM-5 catalysts. *Angew. Chem. Int. Ed.* **51**, 1387–1390.
- Cristiani, C., Bellotto, M., Forzatti, P., and Bregani, F. (1993). On the morphological properties of tungsta-titania de-NO_x catalysts. *J. Mater. Res.* **8**, 2019–2025.
- Custodis, V.B., Hemberger, P., Ma, Z., and van Bokhoven, J.A. (2014). Mechanism of fast pyrolysis of lignin: studying model compounds. *J. Phys. Chem. B* **118**, 8524–8531.
- Dayton, D.C., Carpenter, J.R., Kataria, A., Peters, J.E., Barbee, D., Mante, O.D., and Gupta, R. (2015). Design and operation of a pilot-scale catalytic biomass pyrolysis unit. *Green. Chem.* **17**, 4680–4689.
- Du, Z., Ma, X., Li, Y., Chen, P., Liu, Y., Lin, X., Lei, H., and Ruan, R. (2013). Production of aromatic hydrocarbons by catalytic pyrolysis of microalgae with zeolites: catalyst screening in a pyroprobe. *Bioresour. Technol.* **139**, 397–401.
- Edmunds, C.W., Mukarakate, C., Xu, M., Regmi, Y.N., Hamilton, C., Schaidle, J.A., Labbé, N., and Chmely, S.C. (2019). Vapor-phase stabilization of biomass pyrolysis vapors using mixed-metal oxide catalysts. *ACS Sustain. Chem. Eng.* **7**, 7386–7394.
- Fernández-García, M., and Rodríguez, J.A. (2011). Metal oxide nanoparticles. In *Encyclopedia of Inorganic Bioinorganic Chemistry*, R. Scott, ed. (John Wiley & Sons, Ltd.), pp. 6–7.
- Guntida, A., Suriye, K., Panpranot, J., and Praserthdam, P. (2019). Lewis acid transformation to Bronsted acid sites over supported tungsten oxide catalysts containing different surface WO_x structures. *Catal. Today*.
- Gutiérrez-Alejandre, A., Ramírez, J., and Busca, G. (1998). A vibrational and spectroscopic study of WO₃/TiO₂–Al₂O₃ catalyst precursors. *Langmuir* **14**, 630–639.
- Hemberger, P., Custodis, V.B.F., Bodi, A., Gerber, T., and van Bokhoven, J.A. (2017). Understanding the mechanism of catalytic fast pyrolysis by unveiling reactive intermediates in heterogeneous catalysis. *Nat. Commun.* **8**, 15946.
- Hoff, T.C., Gardner, D.W., Thilakarathne, R., Proano-Aviles, J., Brown, R.C., and Tessonier, J.-P. (2017). Elucidating the effect of desilication on aluminum-rich ZSM-5 zeolite and its consequences on biomass catalytic fast pyrolysis. *Appl. Catal. A Gen.* **529**, 68–78.
- Huber, G.W., Iborra, S., and Corma, A. (2006). Synthesis of transportation fuels from biomass: chemistry, catalysts, and engineering. *Chem. Rev.* **106**, 4044–4098.
- Iliopoulou, E.F., Stefanidis, S.D., Kalogiannis, K.G., Delimitis, A., Lappas, A.A., and Triantafyllidis, K.S. (2012). Catalytic upgrading of biomass pyrolysis vapors using transition metal-modified ZSM-5 zeolite. *Appl. Catal. B Environ.* **127**, 281–290.
- Jae, J., Tompsett, G.A., Foster, A.J., Hammond, K.D., Auerbach, S.M., Lobo, R.F., and Huber, G.W. (2011). Investigation into the shape selectivity of zeolite catalysts for biomass conversion. *J. Catal.* **279**, 257–268.
- Jan, O., Marchand, R., Anjos, L.C.A., Seufitelli, G.V.S., Nikolla, E., and Resende, F.L.P. (2015). Hydrolysis of lignin using Pd/HZSM-5. *Energy Fuels* **29**, 1793–1800.
- Jia, L.Y., Raad, M., Hamieh, S., Toufaily, J., Hamieh, T., Bettahar, M.M., Mauviel, G., Tarrighi, M., Pinard, L., and Dufour, A. (2017). Catalytic fast pyrolysis of biomass: superior selectivity of hierarchical zeolites to aromatics. *Green Chem.* **19**, 5442–5459.
- Kelkar, S., Saffron, C.M., Andreassi, K., Li, Z., Murkute, A., Miller, D.J., Pinnavaia, T.J., and Kriegel, R.M. (2015). A survey of catalysts for aromatics from fast pyrolysis of biomass. *Appl. Catal. B Environ.* **174–175**, 85–95.
- Kim, J.-Y., Lee, J.H., Park, J., Kim, J.K., An, D., Song, I.K., and Choi, J.W. (2015). Catalytic pyrolysis of lignin over HZSM-5 catalysts: effect of various parameters on the production of aromatic hydrocarbon. *J. Anal. Appl. Pyrol.* **114**, 273–280.
- Kim, J., Sarma, B.B., Andrés, E., Pfänder, N., Concepción, P., and Prieto, G. (2019). Surface Lewis acidity of periphery oxide species as a general kinetic descriptor for CO₂ hydrogenation to methanol on supported copper nanoparticles. *ACS Catal.* **9**, 10409–10417.
- Kubiak, C.P. (1995). Preconversion catalytic deoxygenation of phenolic functional groups. *Quarterly technical progress report, July 1, 1995–September 30, 1995* (Purdue Univ., Lafayette, IN (United States). Dept. of Chemistry).
- Koodali, R. (2006). *Catalysis by metal oxides*. In *Surface and Nanomolecular Catalysis*, R. Richards, ed. (CRC press), pp. 48–50.
- Kusumoto, S., and Nozaki, K. (2015). Direct and selective hydrogenolysis of arenes and aryl methyl ethers. *Nat. Commun.* **6**, 6296.
- Li, C., Zhao, X., Wang, A., Huber, G.W., and Zhang, T. (2015a). Catalytic transformation of lignin for the production of chemicals and fuels. *Chem. Rev.* **115**, 11559–11624.
- Li, C.Z., Zheng, M.Y., Wang, A.Q., and Zhang, T. (2012). One-pot catalytic hydrocracking of raw woody biomass into chemicals over supported carbide catalysts: simultaneous conversion of cellulose, hemicellulose and lignin. *Energy Environ. Sci.* **5**, 6383–6390.
- Li, J., Yu, Y., Li, X., Wang, W., Yu, G., Deng, S., Huang, J., Wang, B., and Wang, Y. (2015b). Maximizing carbon efficiency of petrochemical production from catalytic co-pyrolysis of biomass and plastics using gallium-containing MFI zeolites. *Appl. Catal. B Environ.* **172–173**, 154–164.
- Lin, Y.C., Cho, J., Tompsett, G.A., Westmoreland, P.R., and Huber, G.W. (2009). Kinetics and mechanism of cellulose pyrolysis. *J. Phys. Chem. C* **113**, 20097–20107.
- Liu, C., Hu, J., Zhang, H., and Xiao, R. (2016). Thermal conversion of lignin to phenols: relevance between chemical structure and pyrolysis behaviors. *Fuel* **182**, 864–870.
- Liu, C., Wang, H., Karim, A.M., Sun, J., and Wang, Y. (2014). Catalytic fast pyrolysis of lignocellulosic biomass. *Chem. Soc. Rev.* **43**, 7594–7623.
- Liu, G., Wright, M.M., Zhao, Q., and Brown, R.C. (2015). Catalytic fast pyrolysis of duckweed: effects of pyrolysis parameters and optimization of aromatic production. *J. Anal. Appl. Pyrol.* **112**, 29–36.
- Lu, Q., Dong, C.-q., Zhang, X.-m., Tian, H.-y., Yang, Y.-p., and Zhu, X.-f. (2011). Selective fast pyrolysis of biomass impregnated with ZnCl₂ to produce furfural: analytical Py-GC/MS study. *J. Anal. Appl. Pyrol.* **90**, 204–212.
- Lu, Q., Wang, Z.-x., Guo, H.-q., Li, K., Zhang, Z.-x., Cui, M.-s., and Yang, Y.-p. (2019). Selective preparation of monocyclic aromatic hydrocarbons from ex-situ catalytic fast pyrolysis of pine over Ti(SO₄)₂-Mo₂N/HZSM-5 catalyst. *Fuel* **243**, 88–96.
- Luo, Z., Lu, K., Yang, Y., Li, S., and Li, G. (2019). Catalytic fast pyrolysis of lignin to produce aromatic hydrocarbons: optimal conditions and reaction mechanism. *RSC Adv.* **9**, 31960–31968.
- Lup, A.N.K., Abnisa, F., Daud, W.M.A.W., and Aroua, M.K. (2017). A review on reaction mechanisms of metal-catalyzed deoxygenation process in bio-oil model compounds. *Appl. Catal. A Gen.* **541**, 87–106.
- Meng, Q., Hou, M., Liu, H., Song, J., and Han, B. (2017). Synthesis of ketones from biomass-derived feedstock. *Nat. Commun.* **8**, 14190.
- Müller, S., Liu, Y., Kirchberger, F.M., Tonigold, M., Sanchez-Sanchez, M., and Lercher, J.A. (2016). Hydrogen transfer pathways during zeolite catalyzed methanol conversion to hydrocarbons. *J. Am. Chem. Soc.* **138**, 15994–16003.
- Murugappan, K., Mukarakate, C., Budhi, S., Shetty, M., Nimlos, M.R., and Román-Leshkov, Y. (2016). Supported molybdenum oxides as effective catalysts for the catalytic fast pyrolysis of lignocellulosic biomass. *Green Chem.* **18**, 5548–5557.
- Nolte, M.W., Zhang, J., and Shanks, B.H. (2016). Ex situ hydrodeoxygenation in biomass pyrolysis using molybdenum oxide and low pressure hydrogen. *Green Chem.* **18**, 134–138.
- Patwardhan, P.R., Brown, R.C., and Shanks, B.H. (2011). Product distribution from the fast pyrolysis of hemicellulose. *ChemSuschem* **4**, 636–643.
- Patwardhan, P.R., Satrio, J.A., Brown, R.C., and Shanks, B.H. (2010). Influence of inorganic salts on the primary pyrolysis products of cellulose. *Bioresour. Technol.* **101**, 4646–4655.
- Qi, Z., Zhang, B., Ji, J., Li, X., Dai, T., Guo, H., Wang, A., Lu, L., and Li, C. (2018). Selective cleavage of C–O bonds in lignin catalyzed by rhenium (VII) oxide (Re₂O₇). *ChemPlusChem*.

- Rahimi, A., Ulbrich, A., Coon, J.J., and Stahl, S.S. (2014). Formic-acid-induced depolymerization of oxidized lignin to aromatics. *Nature* 515, 249.
- Robinson, A., Ferguson, G.A., Gallagher, J.R., Cheah, S., Beckham, G.T., Schaidle, J.A., Hensley, J.E., and Medlin, J.W. (2016). Enhanced hydrodeoxygenation of m-cresol over bimetallic Pt–Mo catalysts through an oxophilic metal-induced tautomerization pathway. *ACS Catal.* 6, 4356–4368.
- Rogers, K.A., and Zheng, Y. (2016). Selective deoxygenation of biomass-derived bio-oils within hydrogen-modest environments: a review and new insights. *Chemsuschem* 9, 1750–1772.
- Roman-Leshkov, Y., Barrett, C.J., Liu, Z.Y., and Dumesic, J.A. (2007). Production of dimethylfuran for liquid fuels from biomass-derived carbohydrates. *Nature* 447, 982–U985.
- Sanna, A., and Andrésen, J.M. (2012). Bio-oil deoxygenation by catalytic pyrolysis: new catalysts for the conversion of biomass into densified and deoxygenated bio-oil. *ChemSusChem* 5, 1944–1957.
- Schlaf, M., and Zhang, Z.C. (2015). Reaction Pathways and Mechanisms in Thermocatalytic Biomass Conversion II: Homogeneously Catalyzed Transformations, Acrylics from Biomass, Theoretical Aspects, Lignin Valorization and Pyrolysis Pathways (Springer).
- Shao, Y., Xia, Q.N., Dong, L., Liu, X.H., Han, X., Parker, S.F., Cheng, Y.Q., Daemen, L.L., Ramirez-Cuesta, A.J., Yang, S.H., et al. (2017). Selective production of arenes via direct lignin upgrading over a niobium-based catalyst. *Nat. Commun.* 8, 16104.
- Shen, D., and Gu, S. (2009). The mechanism for thermal decomposition of cellulose and its main products. *Bioresour. Technol.* 100, 6496–6504.
- Shiramizu, M., and Toste, F.D. (2012). Deoxygenation of biomass-derived feedstocks: oxorhenium-catalyzed deoxydehydration of sugars and sugar alcohols. *Angew. Chem. Int. Ed.* 51, 8082–8086.
- Teles, C.A., de Souza, P.M., Rabelo-Neto, R.C., Griffin, M.B., Mukarakate, C., Orton, K.A., Resasco, D.E., and Noronha, F.B. (2018). Catalytic upgrading of biomass pyrolysis vapors and model compounds using niobia supported Pd catalyst. *Appl. Catal. B Environ.* 238, 38–50.
- Thilakarathne, R., Tessonier, J.-P., and Brown, R.C. (2016). Conversion of methoxy and hydroxyl functionalities of phenolic monomers over zeolites. *Green Chem.* 18, 2231–2239.
- Vishwanathan, V., Balakrishna, G., Rajesh, B., Jayasri, V., Sikhivihilu, L.M., and Coville, N.J. (2008). Alkylation of catechol with methanol to give guaiacol over sulphate-modified zirconia solid acid catalysts: the influence of structural modification of zirconia on catalytic performance. *Catal. Commun.* 9, 2422–2427.
- Vuori, A.I., and Bredenberg, J.B.-s. (1987). Thermal chemistry pathways of substituted anisoles. *Ind. Eng. Chem. Res.* 26, 359–365.
- Wan, W., Ammal, S.C., Lin, Z., You, K.-E., Heyden, A., and Chen, J.G. (2018). Controlling reaction pathways of selective C–O bond cleavage of glycerol. *Nat. Commun.* 9, 4612.
- Wang, K., Kim, K.H., and Brown, R.C. (2014). Catalytic pyrolysis of individual components of lignocellulosic biomass. *Green Chem.* 16, 727–735.
- Wang, K., Zhang, J., Shanks, B.H., and Brown, R.C. (2015a). The deleterious effect of inorganic salts on hydrocarbon yields from catalytic pyrolysis of lignocellulosic biomass and its mitigation. *Appl. Energy* 148, 115–120.
- Wang, S., Cao, B., Liu, X., Xu, L., Hu, Y., Afonaa-Mensah, S., Abomohra, A.E.-F., He, Z., Wang, Q., and Xu, S. (2018). A comparative study on the quality of bio-oil derived from green macroalgae *Enteromorpha clathrata* over metal modified ZSM-5 catalysts. *Bioresour. Technol.* 256, 446–455.
- Wang, S., Dai, G., Yang, H., and Luo, Z. (2017). Lignocellulosic biomass pyrolysis mechanism: a state-of-the-art review. *Prog. Energy. Combust.* 62, 33–86.
- Wang, S., Guo, X., Liang, T., Zhou, Y., and Luo, Z. (2012). Mechanism research on cellulose pyrolysis by Py-GC/MS and subsequent density functional theory studies. *Bioresour. Technol.* 104, 722–728.
- Wang, S., Ru, B., Lin, H., Sun, W., and Luo, Z. (2015b). Pyrolysis behaviors of four lignin polymers isolated from the same pine wood. *Bioresour. Technol.* 182, 120–127.
- Wang, S., Wang, K., Liu, Q., Gu, Y., Luo, Z., Cen, K., and Fransson, T. (2009). Comparison of the pyrolysis behavior of lignins from different tree species. *Biotechnol. Adv.* 27, 562–567.
- Wichterlová, B., Žilková, N., Uvarova, E., Čejka, J., Sarv, P., Paganini, C., and Lercher, J.A. (1999). Effect of Broensted and Lewis sites in ferrierites on skeletal isomerization of n-butenes. *Appl. Catal. A Gen.* 182, 297–308.
- Wu, S., Shen, D., Hu, J., Zhang, H., and Xiao, R. (2016). Cellulose-lignin interactions during fast pyrolysis with different temperatures and mixing methods. *Biomass Bioenerg.* 90, 209–217.
- Xia, Q., Chen, Z., Shao, Y., Gong, X., Wang, H., Liu, X., Parker, S.F., Han, X., Yang, S., and Wang, Y. (2016). Direct hydrodeoxygenation of raw woody biomass into liquid alkanes. *Nat. Commun.* 7, 11162.
- Xiong, J., Luo, Z., Yang, J., Guo, Y., Piyadasa, A., Wang, S., Hoang, S., Fang, Y., Hu, S., Yang, W., et al. (2019). Robust and well-controlled TiO₂–Al₂O₃ binary nanoarray-integrated ceramic honeycomb for efficient propane combustion. *CrystEngComm* 21, 2727–2735.
- Yang, H., Coolman, R., Karanjkar, P., Wang, H., Dornath, P., Chen, H., Fan, W., Conner, W.C., Mountziaris, T.J., and Huber, G. (2017). The effects of contact time and coking on the catalytic fast pyrolysis of cellulose. *Green. Chem.* 19, 286–297.
- Zhang, H., Xiao, R., Huang, H., and Xiao, G. (2009a). Comparison of non-catalytic and catalytic fast pyrolysis of corncob in a fluidized bed reactor. *Bioresour. Technol.* 100, 1428–1434.
- Zhang, H., Xiao, R., Jin, B., Shen, D., Chen, R., and Xiao, G. (2013). Catalytic fast pyrolysis of straw biomass in an internally interconnected fluidized bed to produce aromatics and olefins: effect of different catalysts. *Bioresour. Technol.* 137, 82–87.
- Zhang, H., Xiao, R., Wang, D., Zhong, Z., Song, M., Pan, Q., and He, G. (2009b). Catalytic fast pyrolysis of biomass in a fluidized bed with fresh and spent fluidized catalytic cracking (FCC) catalysts. *Energy Fuels* 23, 6199–6206.

ISCI, Volume 23

Supplemental Information

Controlling Deoxygenation Pathways in Catalytic Fast Pyrolysis of Biomass and Its Components by Using Metal-Oxide Nanocomposites

Anqing Zheng, Zhen Huang, Guoqiang Wei, Kun Zhao, Liqun Jiang, Zengli Zhao, Yuanyu Tian, and Haibin Li

Supplemental Figures

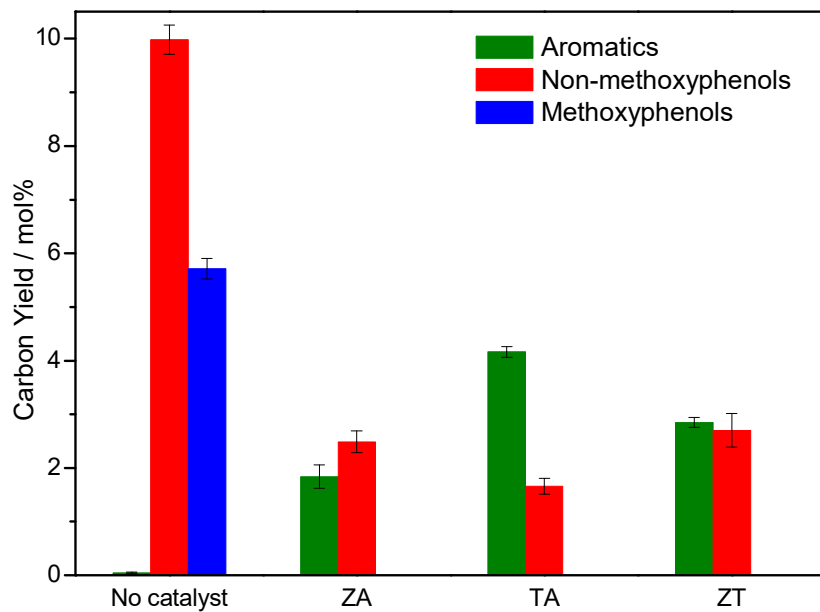


Figure S1 The carbon yields of aromatics and phenols from catalytic fast pyrolysis of organosolv lignin derived from bagasse over different nanocomposites, related to Figure 4.

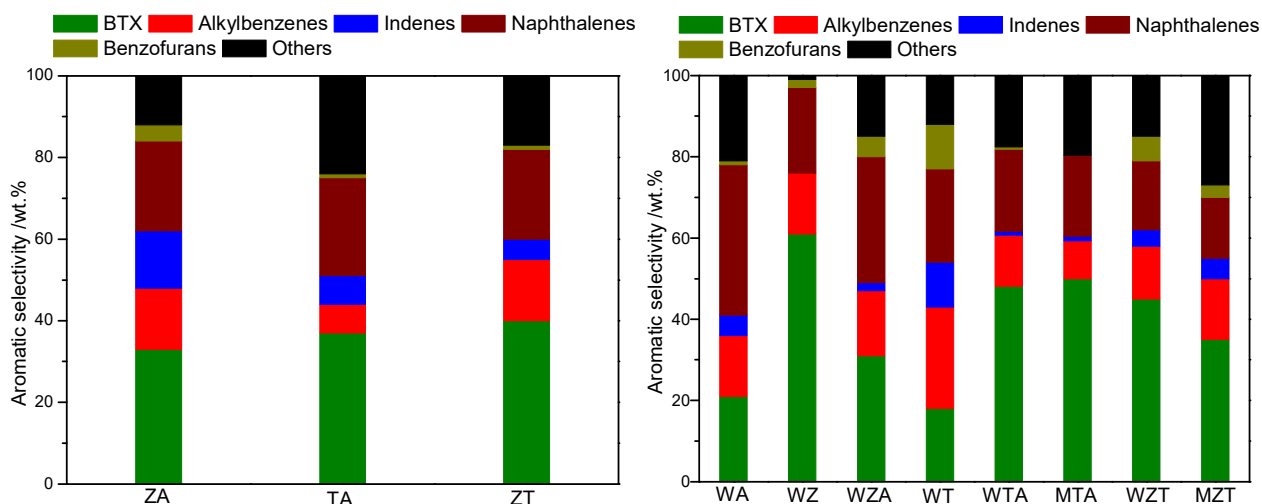


Figure S2 The aromatic selectivity from catalytic fast pyrolysis of organosolv lignin derived from bagasse over different nanocomposites, related to Figure 4.

BTX: benzene, toluene and xylenes; Alkylbenzenes: ethylbenzene, ethyltoluenes, ethylxylenes, trimethylbenzenes, tetramethylbenzenes, pentamethylbenzene; Indenes: Indene, methylindenes; Naphthalenes: naphthalene, methylnaphthalenes, ethylnaphthalenes, dimethylnaphthalenes, trimethylnaphthalenes; Benzofurans: benzofuran, methylbenzofurans; Others: fluorene, methylfluorenes, anthracene, methylanthracenes, phenanthrene, methylphenanthrenes.

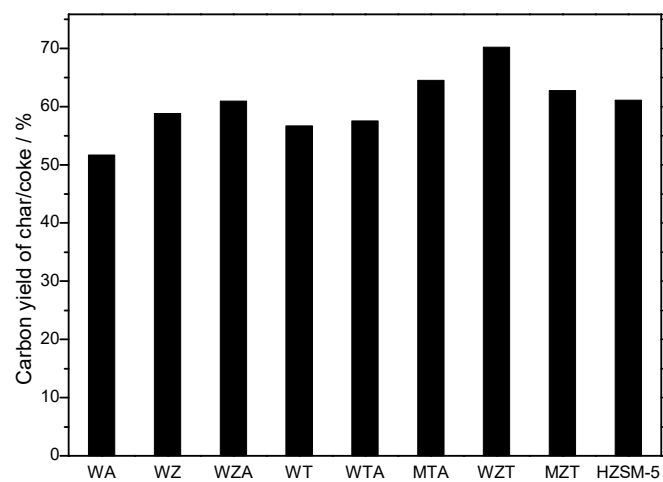


Figure S3 The yields of char/coke from the CFP of organosolv lignin derived from bagasse over different nanocomposites, related to Figure 4.

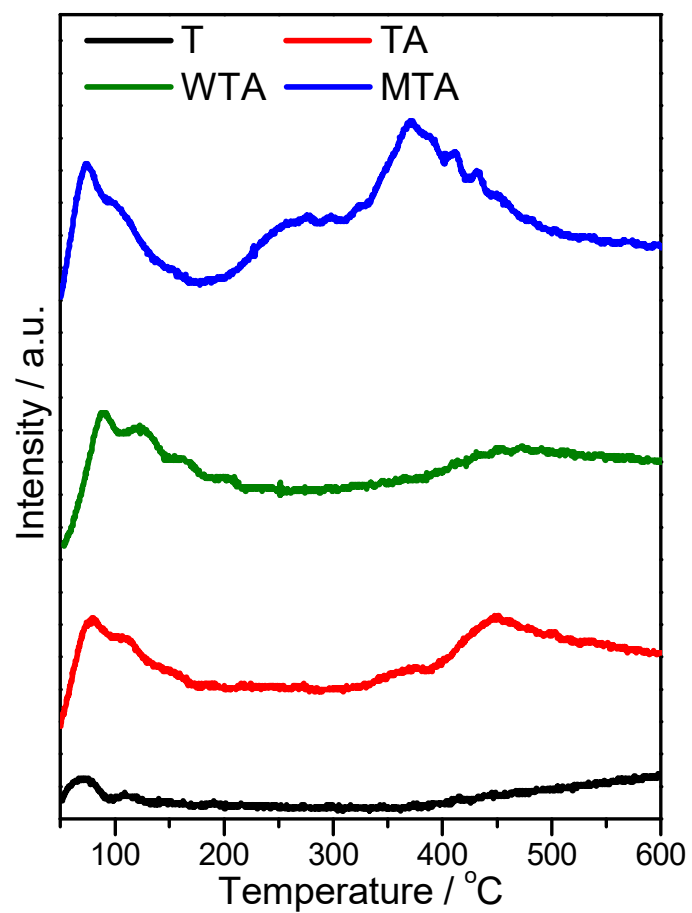


Figure S4 CO₂-TPD profiles of different nanocomposites, related to Figure 7.

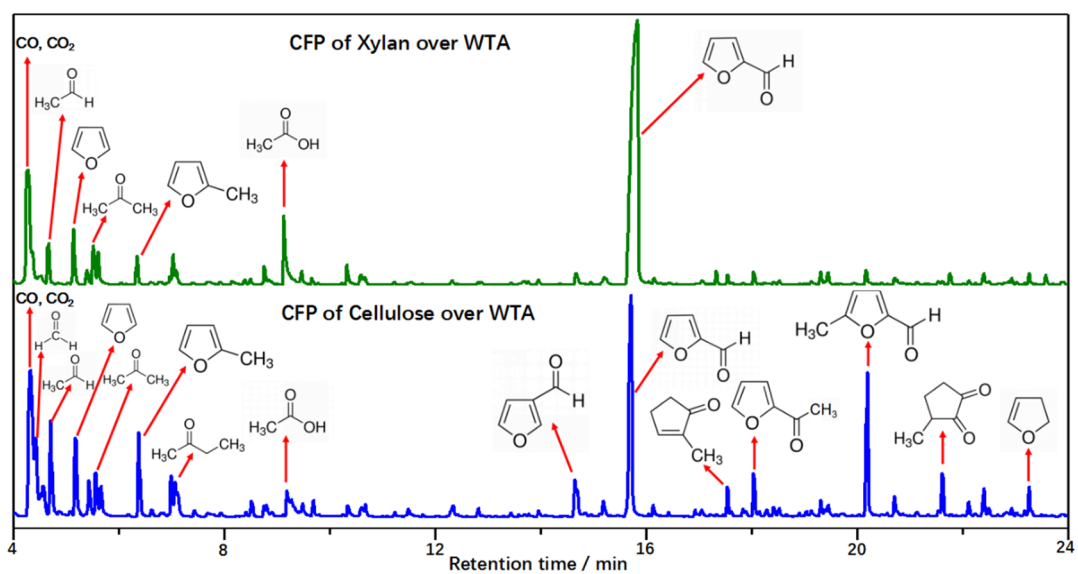


Figure S5 Total ion chromatograms resulting from the CFP of xylan and cellulose over WTA at 600 °C with a catalyst-to-feedstock weight ratio of 3, related to Figure 8.

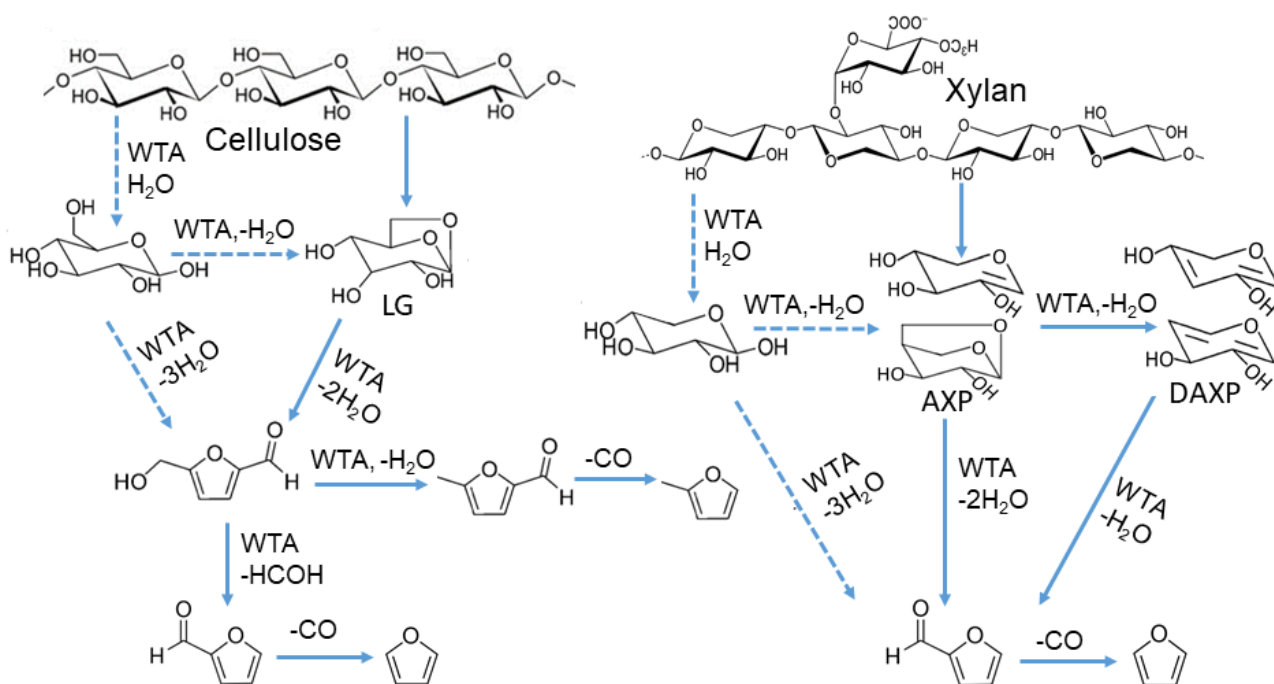


Figure S6 Possible reaction pathways for the formation of furans from the CFP of xylan and cellulose over WTA, related to Figure 8.

Supplemental Tables

Table S1 The yields of aromatics from the CFP of biomass and its components in literature, related to Figure 4 and Figure 10.

Feedstocks	Catalyst	Carbon yield of aromatics	Reference
Lignin	HZSM-5	2-9%	(Wang et al., 2014)
Lignin	CoO/MoO ₃ and HZSM-5	Up to 6.2%	(Mullen and Boateng, 2010)
Lignin, cellulose and biomass	HZSM-5 and H-Beta	1-14%	(Mihalcik et al., 2011)
Red oak	HZSM-5	14.5-17.7%	(Wang et al., 2015)
Lignin	HZSM-5	13.38-27.91% (relative peak area)	(Lee et al., 2016)
Pine	MoO ₃ /TiO ₂	7%	(Murugappan et al., 2016)
Pine	Ti(SO ₄) ₂ -Mo ₂ N/HZSM-5, Mo ₂ N/HZSM-5	Up to 13.63 wt.%	(Lu et al., 2019)
Pine	ZnAl, Zn ₂ Al, MgAl, Mg ₂ Al	Up to 4% (relative peak area)	(Edmunds et al., 2019)
Lignin and biomass	WO ₃ -TiO ₂ -Al ₂ O ₃	Up to 8.5% for lignin and 14.7% for pine	This work

Table S2 The yields of furans from the CFP of biomass and its components in literature, related to Figure 8 and Figure 10.

Feedstocks	Catalyst	Yield of furfural or furans	Reference
Corncoobs	Fe ₂ (SO ₄) ₃ , H ₂ SO ₄ , ZnCl ₂	5–6 wt.%%	(Branca et al., 2012)
Corncoobs	H ₂ SO ₄	0.65-5% wt.%	(Branca et al., 2011)
Biomass, cellulose, and xylan	ZnCl ₂	Up to 70% (relative peak area)	(Lu et al., 2011)
Bagasse	CuSO ₄ /HZSM-5	28% (relative peak area)	(Zhang et al., 2014)
Cellulose	ZrCu-SAPO-18 ZrCu-SAPO-34	Selectivity of 63.86% (relative peak area)	(Chen et al., 2018)
Xylan, cellulose and biomass	WO ₃ -TiO ₂ -Al ₂ O ₃	Up to 29.9% for xylan, 17.7% for cellulose and 20.5% for eucalyptuses (carbon yield)	This work

Transparent Methods

Preparation and characterization

The metal-oxide nanocomposites were synthesized by a coprecipitation method. A stable aqueous TiCl_4 solution was prepared by dissolving the desired amount of TiCl_4 in deionized water with vigorous stirring in an ice-water bath. The W- or Mo-free nanocomposites were precipitated from a mixture of $\text{Al}(\text{NO}_3)_3 \cdot 9\text{H}_2\text{O}$, TiCl_4 or $\text{ZrOCl}_2 \cdot 8\text{H}_2\text{O}$ with different metal-to-metal molar ratios (1:1 for a binary mixture and 1:1:1 for a ternary mixture) by increasing the pH to 9~10 with a 25~28% solution of ammonium hydroxide under vigorous stirring. For the W or Mo-containing nanocomposites, the desired amount of ammonium metatungstate (or ammonium molybdate) was dissolved in the mixture with vigorous stirring before precipitation. The loading of WO_3 or MO_3 was 16 wt.% based on the weights of the other metal oxides. The resulting precipitates were aged at room temperature for 24 h. After filtration and washing, the obtained nanocomposites were dried at 105 °C for 12 h, followed by calcination in air at 600 °C for 2 h. Nanosized TiO_2 and ZrO_2 were purchased from Aladdin Industrial Corporation (Shanghai, China). The commercial HZSM-5 catalyst (Si/Al=25) was obtained from the Catalyst Plant of Nankai University (Tianjin, China). Transmission electron micrographs of the nanocomposites were carried out on a transmission electron microscope (TEM-100CX, JEOL Inc., Tokyo, Japan) at a 200 kV accelerating voltage. Powder X-ray diffraction (XRD) patterns of the nanocomposites were analyzed by an X-ray diffractometer (X'Pert Pro MPD, PANalytical B.V., Almelo, Netherlands) using $\text{Cu K}\alpha$ radiation ($\lambda = 1.54060 \text{ \AA}$) at 40 kV and 40 mA. The diffraction patterns were registered from $2\theta = 5\text{--}80^\circ$ at a scanning rate of 2° min^{-1} . The crystalline phases of metal-oxide nanocomposites were identified by comparison with JCPDS files. Total acid amounts of the nanocomposites were determined by temperature-programmed desorption of NH_3 (NH_3 -TPD)

(DAS-7000, Huasi Instrument Co. Ltd., Changsha, China) connected with a thermal conductivity detector (TCD), and the types of the acid sites and the Brønsted to Lewis acid site ratio of the nanocomposites were determined by the adsorption of pyridine followed by the recording of their Fourier transform infrared (FTIR) spectra on a Frontier spectrometer (PerkinElmer Inc., Boston, USA), the concentrations of Brønsted and Lewis acid sites were subsequently calculated according to the method described by literature (Emeis, 1993; Tamura et al., 2012; Weingarten et al., 2011). The temperature-programmed measurements for the desorption of CO₂ (CO₂-TPD) of the nanocomposites were performed in a DAS-7000 (Huasi Instrument Co. Ltd., Changsha, China).

Catalytic fast pyrolysis and product analysis

Xylan and cellulose were purchased from Macklin Inc. (Shanghai, China) and Sigma–Aldrich (St Louis, USA), respectively. Organosolv lignin was extracted from bagasse by organosolv fractionation according to our previous studies (Zheng et al., 2017; Zheng et al., 2018). Catalytic fast pyrolysis of the biomass and its major components was conducted in a commercial micropyrolyzer (Pyroprobe 5200, CDS Analytical, Oxford, PA, USA). The samples were mixed with nanocomposites in an agate mortar to ensure thorough mixing. A mixture with the desired catalyst-to-feedstock weight ratio was accurately weighed on an analytical balance to an accuracy of 0.001 mg (XP6152, Mettler-Toledo GmbH, Giessen, Germany), and the pyrolysis temperature, residence time, and heating rate were fixed to 600 °C, 20 s, and 10,000 K/s, respectively. The pyrolysis products were analyzed in-line by an Agilent 7890 series gas chromatograph (GC) coupled with an Agilent 5975 series mass-selective detector (MSD). The GC column used was a J&W DB1701 column with dimensions of 60 m × 250 μm × 0.25 μm. The major pyrolysis products were quantified using the external standard method according to the guidelines provided by Agilent. The calibration curves were obtained by injecting the

mixed standard solutions with at least five concentrations of the target compounds into the GC oven under the same operating conditions. The carbon yields of the target products from the CFP of lignin, xylan or cellulose are defined as the moles of carbon in the target products divided by the moles of carbon in the feedstocks. The carbon yields of the furans from the raw biomass were calculated by the moles of carbon in the furans divided by the moles of carbon in the hemicellulose and cellulose fractions of the raw biomass. The carbon yields of the aromatics or phenols from the CFP of the raw biomass were calculated by the moles of carbon in the aromatics or phenols divided by the moles of carbon in the lignin fraction of the raw biomass. The carbon yields of char/coke were obtained by the elemental analysis of spent catalysts.

Supplemental References

- Branca, C., Di Blasi, C., and Galgano, A. (2012). Catalyst Screening for the Production of Furfural from Corn cob Pyrolysis. *Energy Fuel* 26, 1520-1530.
- Branca, C., Galgano, A., Blasi, C., Esposito, M., and Di Blasi, C. (2011). H₂SO₄-Catalyzed Pyrolysis of Corncobs. *Energy Fuel* 25, 359-369.
- Chen, X., Chen, Y., Chen, Z., Zhu, D., Yang, H., Liu, P., Li, T., and Chen, H. (2018). Catalytic fast pyrolysis of cellulose to produce furan compounds with SAPO type catalysts. *J Anal Appl Pyrol* 129, 53-60.
- Edmunds, C.W., Mukarakate, C., Xu, M., Regmi, Y.N., Hamilton, C., Schaidle, J.A., Labbé, N., and Chmely, S.C. (2019). Vapor-Phase Stabilization of Biomass Pyrolysis Vapors Using Mixed-Metal Oxide Catalysts. *ACS Sustain Chem Eng* 7, 7386-7394.
- Emeis, C. (1993). Determination of integrated molar extinction coefficients for infrared absorption bands of pyridine adsorbed on solid acid catalysts. *J Catal* 141, 347-354.
- Lee, H.W., Kim, Y.-M., Jae, J., Sung, B.H., Jung, S.-C., Kim, S.C., Jeon, J.-K., and Park, Y.-K. (2016). Catalytic pyrolysis of lignin using a two-stage fixed bed reactor comprised of in-situ natural zeolite and ex-situ HZSM-5. *J Anal Appl Pyrol* 122, 282-288.
- Lu, Q., Dong, C.-q., Zhang, X.-m., Tian, H.-y., Yang, Y.-p., and Zhu, X.-f. (2011). Selective fast pyrolysis of biomass impregnated with ZnCl₂ to produce furfural: Analytical Py-GC/MS study. *J Anal Appl Pyrol* 90, 204-212.
- Lu, Q., Wang, Z.-x., Guo, H.-q., Li, K., Zhang, Z.-x., Cui, M.-s., and Yang, Y.-p. (2019). Selective preparation of monocyclic aromatic hydrocarbons from ex-situ catalytic fast pyrolysis of pine over Ti(SO₄)₂-Mo₂N/HZSM-5 catalyst. *Fuel* 243, 88-96.
- Mihalcik, D.J., Mullen, C.A., and Boateng, A.A. (2011). Screening acidic zeolites for catalytic fast pyrolysis of biomass and its components. *J Anal Appl Pyrol* 92, 224-232.
- Mullen, C.A., and Boateng, A.A. (2010). Catalytic pyrolysis-GC/MS of lignin from several sources. *Fuel Process Technol* 91, 1446-1458.

- Murugappan, K., Mukarakate, C., Budhi, S., Shetty, M., Nimlos, M.R., and Román-Leshkov, Y. (2016). Supported molybdenum oxides as effective catalysts for the catalytic fast pyrolysis of lignocellulosic biomass. *Green Chem* *18*, 5548-5557.
- Tamura, M., Shimizu, K.-i., and Satsuma, A. (2012). Comprehensive IR study on acid/base properties of metal oxides. *Appl Catal A-Gen* *433-434*, 135-145.
- Wang, K., Kim, K.H., and Brown, R.C. (2014). Catalytic pyrolysis of individual components of lignocellulosic biomass. *Green Chem* *16*, 727-735.
- Wang, K., Zhang, J., Shanks, B.H., and Brown, R.C. (2015). The deleterious effect of inorganic salts on hydrocarbon yields from catalytic pyrolysis of lignocellulosic biomass and its mitigation. *Appl Energy* *148*, 115-120.
- Weingarten, R., Tompsett, G.A., Conner Jr, W.C., and Huber, G.W. (2011). Design of solid acid catalysts for aqueous-phase dehydration of carbohydrates: The role of Lewis and Brønsted acid sites. *J Catal* *279*, 174-182.
- Zhang, H., Liu, X., Lu, M., Hu, X., Lu, L., Tian, X., and Ji, J. (2014). Role of Brønsted acid in selective production of furfural in biomass pyrolysis. *Bioresource Technol* *169*, 800-803.
- Zheng, A., Chen, T., Sun, J., Jiang, L., Wu, J., Zhao, Z., Huang, Z., Zhao, K., Wei, G., He, F., *et al.* (2017). Toward fast pyrolysis-based biorefinery: selective production of platform chemicals from biomass by organosolv fractionation coupled with fast pyrolysis. *ACS Sustain Chem Eng* *5*, 6507-6516.
- Zheng, A.Q., Zhao, K., Sun, J.W., Jiang, L.Q., Zhao, Z.L., Huang, Z., Wei, G.Q., He, F., and Li, H.B. (2018). Effect of microwave-assisted organosolv fractionation on the chemical structure and decoupling pyrolysis behaviors of waste biomass. *J Anal Appl Pyrol* *131*, 120-127.